AD-753 275

10-MICROMETERS DETECTOR

W. Chiou, et al

AIL

Prepared for:

Office of Naval Research
Advanced Research Projects Agency

November 1972

SEMIANNUAL REPORT
10-MICROMETERS DETECTOR

ARPA Order No. 1806

Contract No. N00014-70-C-0161
(Modification P00004)

Program Code No. 2E90K21
Investigators: W. Chiou,
M. Aita, and F. Pace
(516) 595-4459

Contractor:
AIL, a division of CUTLER-HAMMER
Deer Park, New York 11729

Scientific Officer:
Director, Physics Programs
Physical Science Division
Office of Naval Research

Effective Date of Contract: 1 December 1969
Contract Expiration Date: 31 December 1972
Amount of Contract: $276, 724

Sponsored by Advanced Research
Projects Agency, ARPA Order No. 1806

Date: November 1972

This research was supported by the Advanced Research Project Agency of the Department of Defense and was monitored by ONR under Contract No. N00014-70-C-0161.

SEMIANNUAL REPORT
10-MICROMETERS DETECTOR

ARPA Order No. 1806

Contract No. N00014-70-C-0161
(Modification P00004)

Program Code No. 2E90K21
Investigators: W. Chiou,
M. Aita, and F. Pace
(516) 595-4459

Contractor:
AIL, a division of CUTLER-HAMMER
Deer Park, New York 11729

Scientific Officer:
Director, Physics Programs
Physical Science Division
Office of Naval Research

Effective Date of Contract: 1 December 1969
Contract Expiration Date: 31 December 1972
Amount of Contract: $276, 724

Sponsored by Advanced Research
Projects Agency, ARPA Order No. 1806

Date: November 1972

This research was supported by the Advanced Research Project Agency of the Department of Defense and was monitored by ONR under Contract No. N00014-70-C-0161.

TABLE OF CONTENTS

LIST OF ILLUSTRATIONS

I. INTRODUCTION

This document is a semiannual report prepared under Contract N00014-70-C-0161, Modification P00005. The purpose of the program performed under this contract is to continue the research on 10.6 μm image upconversion detectors and to determine the feasibility of developing a 10.6 μm range gated upconversion imaging laser radar receiver with 150 by 150 resolution elements. To meet the program objectives, the following study areas have been required by the contract:

- Experimental determination of the effect of a diverging pump on image resolution for the image space configuration upconverter system, and comparison of the results with analytical prediction.
- Analytical determination of the effect of birefringence and a truncated pump beam on image resolution.
- Development of techniques to handle power dissipation inside the nonlinear crystal.
- Investigation of techniques for improvement of optical efficiency.

During this reporting period an experimental model image upconverter capable of real time direct viewing has been assembled. Imaging characteristics such as resolution, field of view, and the upconversion efficiency of the experimental model were measured by arranging the model in the Fourier space and the image space configurations.

A resolving power of better than 150 by 150 elements has been demonstrated with the Fourier space configuration. The number of resolution

elements obtained with the image space configuration is 65 by 65. The measured angular resolution in both configurations is nearly equal to the diffraction limit. The number of resolution elements obtained with the image space configuration is limited by the area of usable interaction aperture.

The most important experimental findings with regard to the imaging properties of the image space upconversion are:

- Resolution in the Fourier space configuration is degraded by the pump beam amplitude distribution.
- Resolvable image linewidth of the image space configuration agrees closely with the prediction based on the physical optics analysis. The geometric optics estimate is three to four times poorer than the measured results.
- Resolution in the image space configuration would not be affected by the pump beam intensity profile. An effect of the pump beam intensity distribution appears as nonuniform intensity across the image plane.
- Use of a diverging multimode pump beam does not degrade image resolution if the upconverter is in the image space configuration.
- Conversion efficiency of the TEM_{oo} mode beam pumped upconverter approaches the estimate (within a factor of three) for perfectly matched plane wave interaction.

The experimental model was also operated in the pulse gated mode. Preliminary results of this experiment are also presented in this report.

Analysis describing the optical transfer function of the Fourier space configuration and the line spread functions of non-Fourier space configuration are presented in Section III. The crystal birefringency is included in the analysis. Calculation of resolving power and some consideration on

the object optics are also included in Section III. The main results of this analysis are:

- The Fourier space configuration image upconverter is indeed free of aberrations. The field of view is limited by the phase matching condition rather than the crystal aperture or the pump beam size.
- Resolving power of the Fourier space configuration upconverter pumped by a Gaussian beam is limited by the diffraction due to the Gaussian aperture when the lens diffraction is negligible.
- Because of the crystal birefringence, the upconverted image of a line object normal to the plane containing the crystal C axis and the pump wave vector consists of several narrow nearly-equal-intensity lines. This fine structure has, however, not been observed experimentally.

Section IV presents measurements of conversion efficiency and realistic estimates of practically achievable efficiency. It is concluded that the conversion efficiency estimation based on the generally accepted plane wave interaction could be achievable at the center of the field of view. Realistic values for the SHG d coefficients of proustite are also considered.

The plans and the areas of study for the remainder of this program are discussed in Section V.

II. REAL TIME IMAGE UPCONVERSION EXPERIMENTS WITH THE DIRECT VIEWING LABORATORY MODEL

An experimental model upconverter capable of real time direct viewing of upconverted images has been set up during this period.

The imaging characteristics of the upconverter were measured first with the proustite crystal pumped by a CW TEM_{oo} mode beam. The resolving power of this model arranged in the Fourier space configuration was measured to assess how close it comes to achieving diffraction limited operation. The model was then set up in the image space configuration to measure the extent of thickness aberration.

The measured angular resolution of approximately 1 milliradian for the Fourier space configuration was within a factor of two of the Rayleigh resolution of a uniformly illuminated object lens aperture. The number of resolution elements contained in a 10-degree field of view, which is also experimentally checked, is consequently better than the resolution objective for the program of 150 by 150 elements. Upconverted images of a 10.6-μm illuminated USAF 1951 resolution chart containing groups smaller than 1 lp/mm were obtained. Because the resolution chart does not fill the field of view, the actual number of resolvable elements contained in the recorded images which fills a 7.5-degree angle is 114 by 114.

The resolving power of the model arranged in the image space configuration was also measured. The experimental results prove (as expected) that the resolvable image linewidth is limited by the thickness aberration. The measured image resolution linewidth of 60 μm agrees with the physical optics prediction of 68 μm, but is approximately three to four times narrower than the geometric optics calculation. The main reason for failure of the geometric optics theory to accurately predict the extent of aberration is probably due to the inability of the geometric optics to account for the intensity variation of the upconverted image rays. Upconverted images of the resolution chart with 62 by 62 resolution elements were obtained with the experimental model in the image space configuration. Measured angular resolution is slightly worse than the diffraction limited angular resolution of the object lens.

The effect of diverging pump beam on the resolving power of the upconverter system in the image space configuration was investigated. The fact that resolution of the image space configuration system using a multimode pump beam does not degrade from that of a TEM_{oo} mode pumped system was verified experimentally. However, a nonuniform intensity corresponding to the multimode pattern is superimposed on the upconverted image.

Image upconversion experiments with the image space configured model, using pulsed pump beam and a gated image tube, were also carried out. Some preliminary results of the experiments are presented in paragraph E of this section.

A. EXPERIMENTAL ARRANGEMENT

The experimental model upconverter system is shown schematically in Figure 1. The system was arranged so that the optical configuration and the pump beam parameters could be readily changed with minimum physical alteration of the setup. A 2.5-cm diameter, and 0.6 cm thick proustite crystal was used. The upconverter was aligned for Type II noncritical phase matching. The proustite was oriented such that its crystallographic X axis lies in the plane of paper and is parallel to the front surface. Its optic axis lies in a plane perpendicular to the paper and makes an angle of 20 degrees with the normal (along the C axis) to the polished front and back surfaces. A continuously pumped Nd:YAG laser radiating electric fields, polarized parallel to the plane of paper, was used as a pump source. The laser is fitted with an acousto-optic Q-switch allowing pulsed as well as CW operation. The beam parameters of the 1.06-μm pump beam emanating out of the beam expander are shown in Table 1 for various modes of operation.

TABLE 1. 1.06-μm PUMP BEAM PARAMETERS AFTER BEAM EXPANSION

MODE	AVERAGE POWER	BEAM CROSS SECTION	BEAM DIAMETER	BEAM DIVERGENCE
CW TEM_{00}	5.0 watts	Gaussian	1.1 cm	0.16 mrad
CW Multi-mode	7.5 watts		1.1 cm	1.0 mrad
Q-Switched TEM_{00} 1000 PPS	0.5 watt	Gaussian	1.1 cm	0.16 mrad

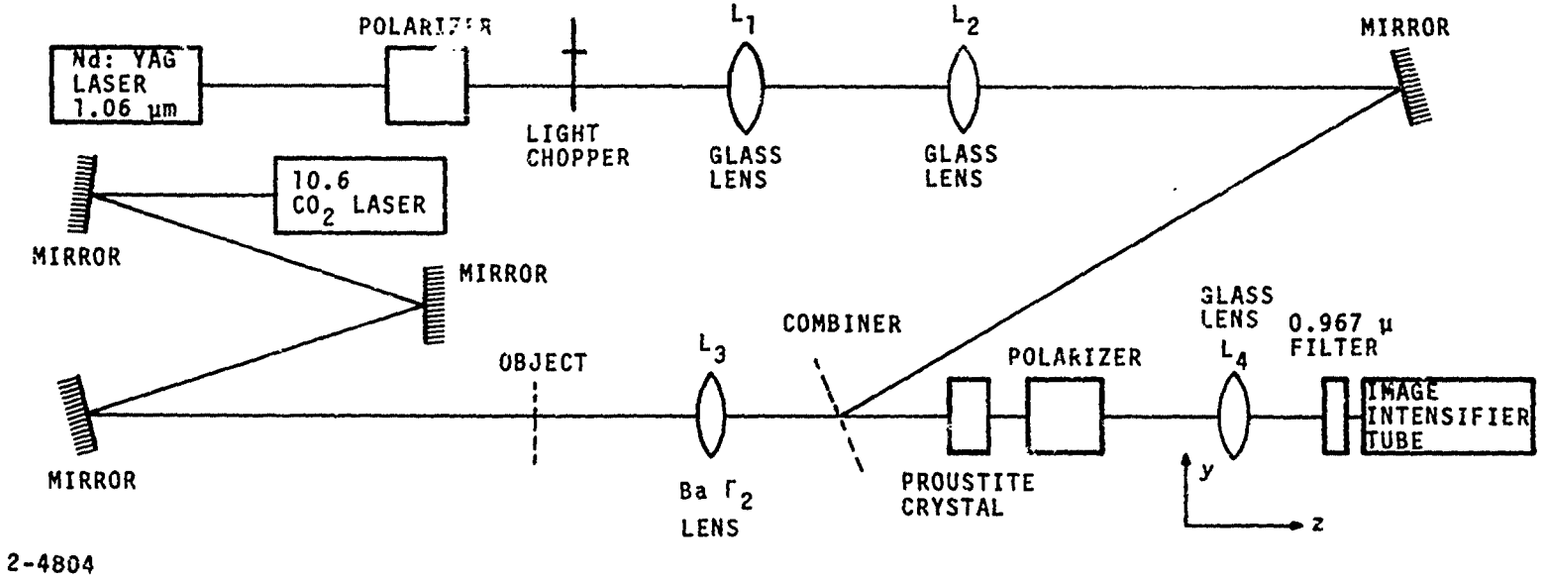

FIGURE 1. SCHEMATIC DIAGRAM, EXPERIMENTAL MODEL IMAGE UPCONVERTER SYSTEM

A polarizer external to the Nd:YAG laser removes field components polarized along the y direction. The chopper reduces the average power of the pump beam by serving as an attenuator when required. Glass lenses L_1 and L_2 collimate and expand the pump beam.

A multimode CO_2 laser radiating with an electric field polarized perpendicular to the plane of the paper was used to back illuminate the transparent 1951 USAF resolution chart. The CO_2 beam diameter at the resolution chart is sufficiently large to illuminate the entire resolution chart by adjusting the 10.6-μm path length by means of mirrors as shown in Figure 1. The position of BaF_2 lens L_3, relative to the proustite crystal and the object, is determined by the configuration of the system (image space or Fourier space).

The pump wave and the object wave are combined by a dichroic mirror. An improved dichroic mirror was obtained during this reporting period. This mirror reflects more than 99 percent of the YAG beam and has a transmission loss at 10.6 μm of about 13 percent. As shown in Figure 1, the angle of incidence of the YAG beam on the dichroic mirror is about 20°. This eliminates potential vignetting of 10.6-μm object waves by the mirror holder.

A Glan air polarization filter and narrowband interference filters are used for suppression of 1.06-μm pump wave. Transmission through these filters at 0.967 μm is about 10 percent. Lens L_4 is used to form

upconverted real images on the photo surface of the image intensifier tube. The image intensifier tube is an ITT Model 4740 three-stage gated tube with an S-1 photocathode. Its pertinent characteristics are listed in Table 2. The image intensifier tube can be cooled to -30°C with dry ice to reduce tube thermal noise.

TABLE 2. CHARACTERISTICS OF ITT MODEL F4740 IMAGE TUBE

Useful Cathode Diameter	23 mm
Radiant Sensitivity at 0.967 μm	1.3 mA/W
Center Resolution	28 lp/mm
Peripheral Resolution	25 lp/mm at 7.0-mm radius
Paraxial Magnification	0.84
Distortion	18 percent at 10-mm radius
Luminous Gain	6000 fL/fc
Conversion Efficiency at 1.06 μm	$1{,}000{,}000 \frac{L(P-20)}{W(1.06)}$
Radiant Power Gain Peak Wavelength	1040 W/W
Radiant Power Gain 1.06 μ	208 W/W
Equivalent Background Energy Input at Peak Wavelength	2×10^{-9} W/cm^2
Equivalent Background Energy Input at 1.06 μ	8×10^{-9} W/cm^2

To check the resolving power of the 0.967 μm image detector used in the system, consisting of lens L_4, the interference filter, the image intensifier tube, and the camera, the resolution chart is illuminated with visible light and imaged on the photosurface of the image intensifier tube. Figure 2 shows a typical image recorded on the film. The smallest

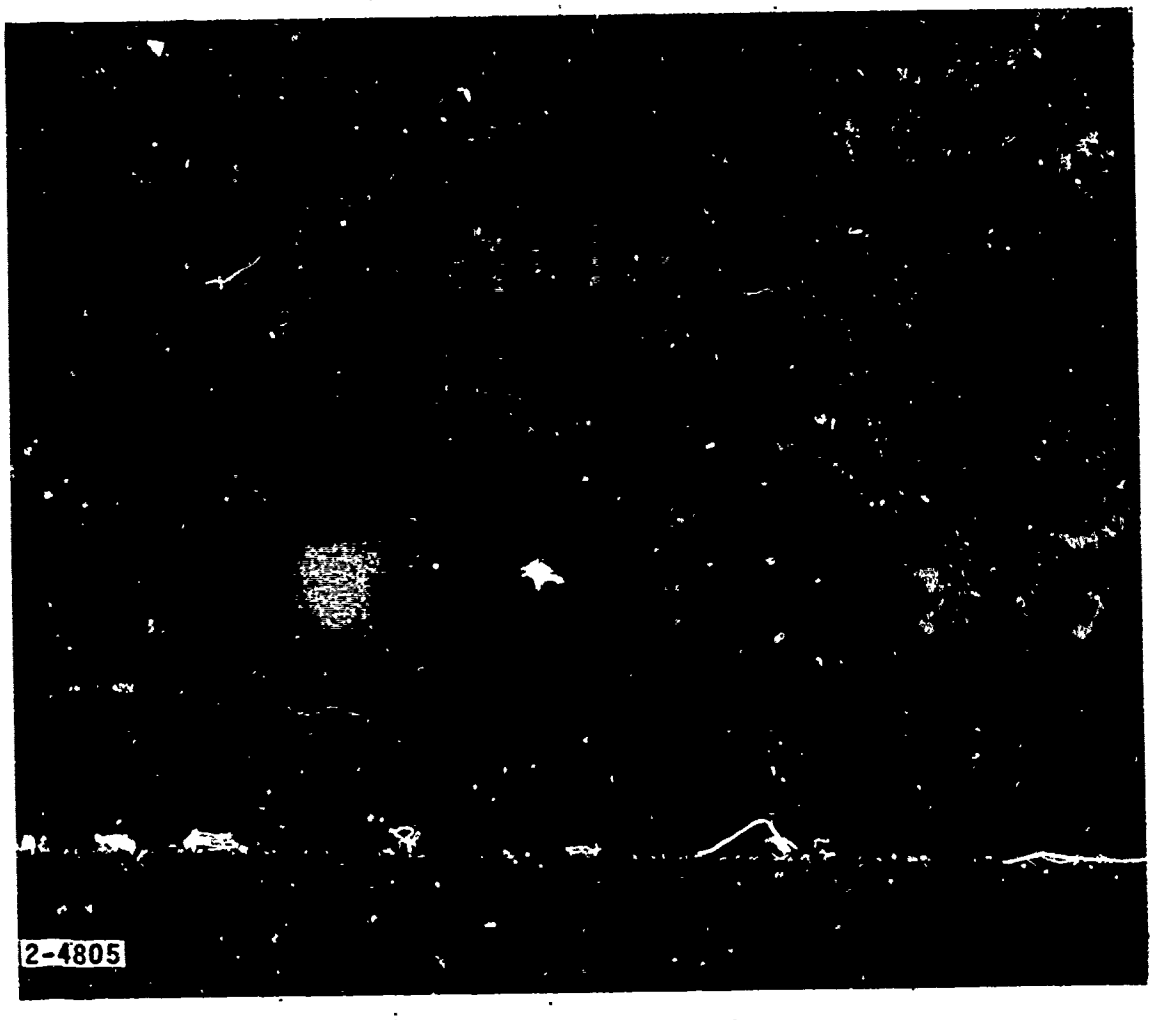

RESOLUTION LIMITS OF THE 0.967-μm IMAGE DETECTOR OF THE EXPERIMENTAL MODEL IS 37 μm AS SEEN IN THE ILLUSTRATION

FIGURE 2. IMAGE OF THE RESOLUTION CHART ILLUMINATED BY VISIBLE LIGHT

resolvable linewidth on the output phosphor of the image tube is 37 μm. A modified polaroid scope camera was used to record the upconverted images produced by the image tube.

B. IMAGE UPCONVERSION IN FOURIER SPACE

The limiting resolving power of the experimental model was measured by operating the model in Fourier Space configuration and pumping the nonlinear material with a TEM_{oo} mode beam. Diffraction limited image upconversion is possible for this configuration if the pump is a plane wave[1]. Thickness aberrations are negligible for this configuration.

A 1951 USAF resolution chart was placed in the front focal plane of lens L_3. The distance between BaF_2 lens L_3 and the proustite crystal is 120 mm which is equal to the focal length of lens L_3. Lens L_4 is placed so that the proustite crystal and the photocathode of the image intensifier tube coincide with the front and back focal planes of lens L_4, respectively. The focal length of lens L_4 is 580 mm.

The pump beam diameter at the proustite front face is 1.1 cm and its beam divergence is 0.16 mrad. The pump beam is in TEM_{oo} transverse mode. Pictures reproduced from some of the upconverted images and recorded by the polaroid camera are shown in Figure 3. The smallest element that can be visually resolved in these figures is the group 2/1. Figure 3A has better resolution along the x direction, but Figure 3B has better resolution along the y direction. (See Figure 1 for the coordinate system.) Inspection

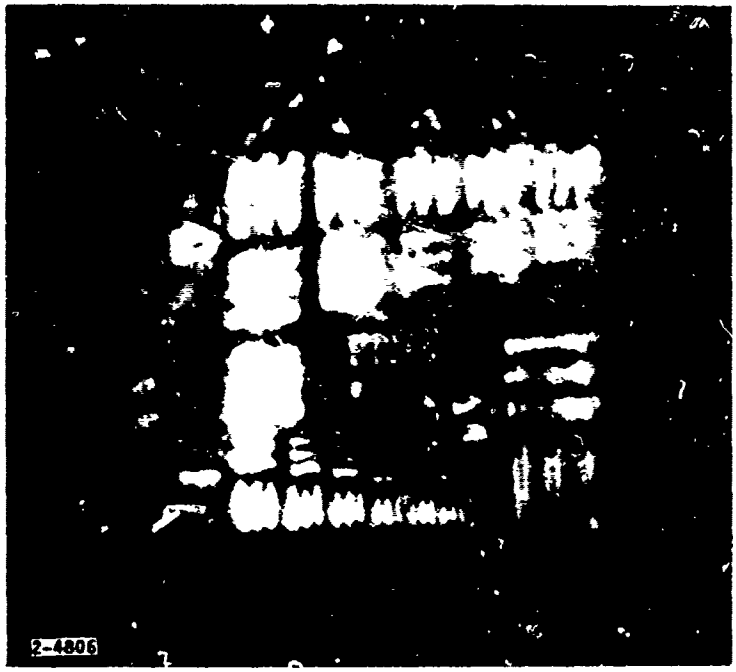

A. BETTER RESOLUTION ALONG X-DIRECTION

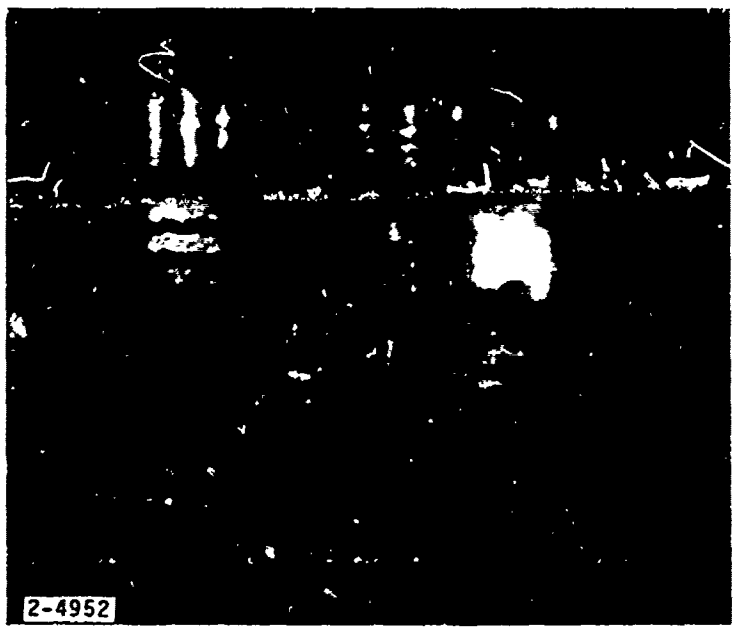

B. BETTER RESOLUTION ALONG Y-DIRECTION

FIGURE 3. UPCONVERTED IMAGE OF 1951 USAF TEST CHART PRODUCED BY FOURIER SPACE UPCONVERTER

of upconverted images on the output phosphor surface of the image intensifier tube indicates that group 1/6 is resolved along both the x and the y directions. The system angular resolution is calculated by the formula

$$\gamma = h_{ir}/f_3 \tag{2-1}$$

where

h_{ir} = resolvable linewidth of the test chart

f_3 = effective focal length of lens L_3

The measured angular resolution corresponding to the 1/6 and 2/1 resolution groups is:

Group 1/6 $h_{ir} = 1/7.13$ mm $= 1.17 \times 10^{-3}$ rad

Group 2/1 $h_{ir} = 1/8$ mm $= 1.04 \times 10^{-3}$ rad

Measured angular resolution of 1.17 mrad is 2.5 times larger than the Rayleigh resolution angle of 3-cm diameter lens L_3.

Resolution degradation from the Rayleigh resolution angle of the object lens is mainly due to nonuniform transverse intensity distribution of the pump beam. It will be shown later that a Gaussian profile of the pump beam would introduce an additional Gaussian attenuation factor on the angular spectrum of the upconverted image field. It is, therefore, expected that the resolving power of the experimental model is limited by the Gaussian window diffraction rather than the object lens diffraction.

The system field of view was measured by translating the object along the x and y directions until the edge of the test chart disappeared. The measured system FOV of 0.183 rad (10.5^{o}) agrees with the previous result[1,2,3]. Figure 3A shows that the FOV covers more than the area occupied by the resolution chart. The number of resolvable elements contained in the FOV is found to be 156 by 156, if one takes group 1/6 as the minimum resolvable element. The image shown in Figure 3A contains approximately 114 by 114 resolution elements.

The measured transverse magnification of 0.99 agrees within 10 percent of the estimated value of 1.08, which is calculated by the expression

$$\left|M\right| = \left|M_{uc}\, M_{c}\, M_{T}\right|$$

where

$M_{uc}\left(= \dfrac{\lambda_s}{\lambda_{ir}}\,\dfrac{f_4}{f_3} = 0.44\right)$: upconversion magnification

M_{c} (= 2.94): camera magnification

M_{T} (= 0.81): image tube magnification

C. IMAGE UPCONVERSION IN IMAGE SPACE

Image upconversion experiments were carried out with the experimental model arranged in the image space configuration. Lens L_3 of Figure 1 was positioned such that a real 10.6-μm image of object is focused

onto the crystal. The photosurface of the image intensifier and the proustite crystal coincide with the conjugate planes of lens L_4.

It has been shown analytically that the resolvable image linewidth of the image space configuration upconverter pumped with a plane wave is limited by thickness aberration[1, 2]. It is the purpose of this experiment to measure the aberrations and to determine the limiting resolution of the image space configured upconverter. The Nd:YAG laser was operated in the TEM_{oo} mode to minimize the effect of diverging pump beam.

Figure 4 shows reproduced pictures of upconverted images recorded by the camera. The magnification of image forming lenses L_3 and L_4 are, respectively, 0.304 and 2.76. The smallest resolvable group (1/3) has a linewidth of 2.52 lp/mm. The corresponding image width, calculated by dividing the resolvable target width by the magnification factor of lens L_3, is 60.3 μm.

An experimentally measured resolvable image linewidth of 60 μm is approximately a factor of 3 narrower than the resolvable image width predicted by the geometric optics calculation. As will be shown in Section III, the physical optics calculation predicts that the minimum resolvable image width for the given parameter values is 68 μm. The experimental result agrees better with the physical optics prediction than with the geometric optics calculation.

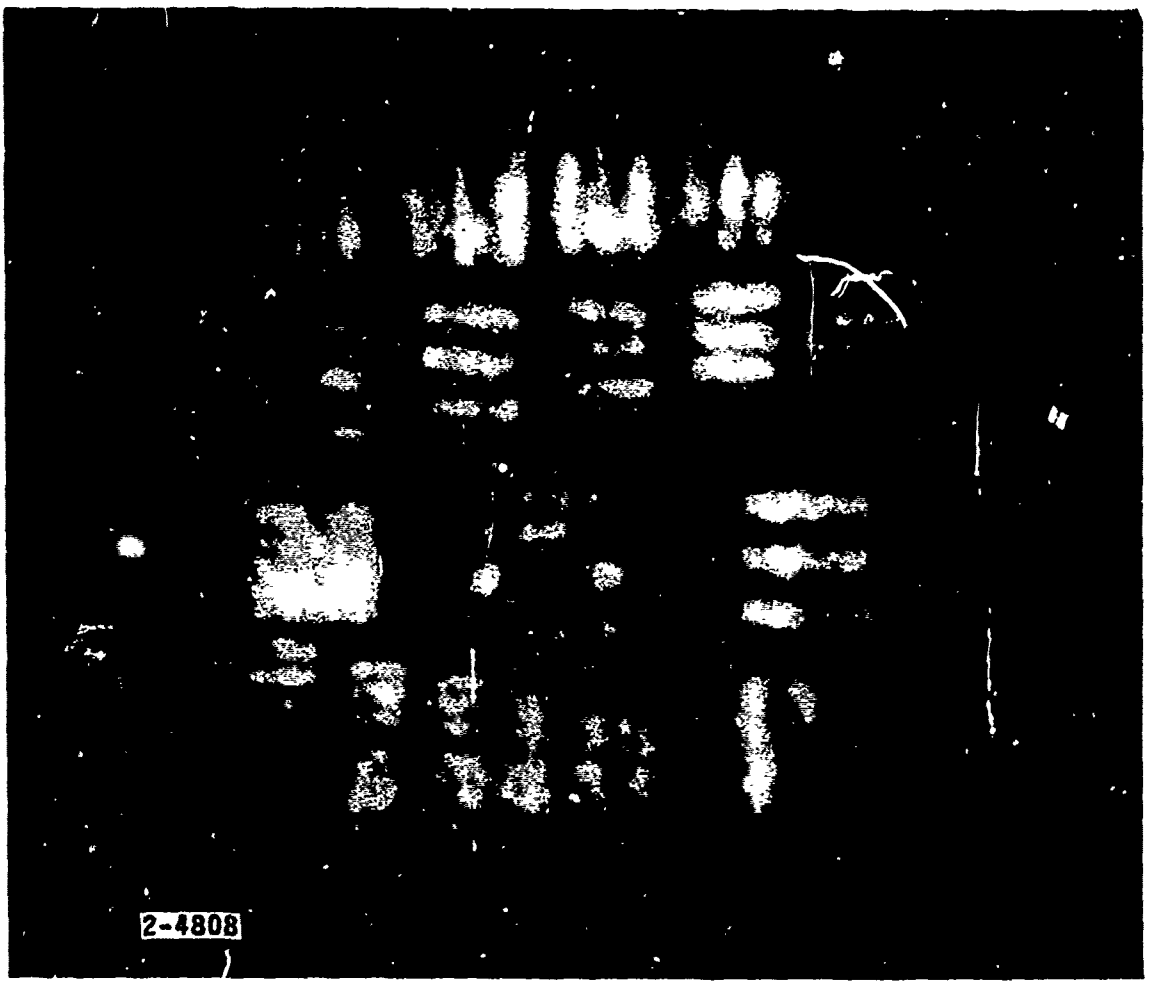

FIGURE 4. UPCONVERTED IMAGE OF 1951 USAF TEST CHART PRODUCED BY IMAGE SPACE UPCONVERTER WITH SINGLE MODE PUMP

In the geometric optics model, the analysis is based on the assumption that each infinitesimal slab of material is capable of forming an independent upconverted image. The concept of thickness aberrations is, therefore, introduced by considering the upconverted image as a congregation of images formed by infinitesimal slabs of upconverter material. It has been previously shown (by the Fourier optics treatment) that the aberration is physically introduced by imperfect phase matching of angular spectra of the interacting electric fields. The angular spectrum with higher spatial frequency suffers higher attenuation due to the phase mismatch. The degree of phase mismatch is proportional to the material thickness. In the physical optics model the upconverted image is formed by linear superposition of the upconverted rays (angular spectra) emanating from the exit surface of the material. It is expected that the aberrations calculated by these two models should be different from each other. The experimental results should agree better with the Fourier optics predictions rather than the geometric optics because the model is in better agreement with the actual physical process.

The number of resolution elements contained in the image shown in Figure 4 is approximately 62 by 62 which is approximately a factor of two less than that obtained by the Fourier space configuration system. Measured system magnification is approximately 10 percent greater than the theoretical estimate.

The system angular resolution can be calculated by dividing the measured resolvable image width by the distance between the crystal and

lens L_3. Measured system angular resolution of 0.4 mrad is very close to the Rayleigh resolution angle of 0.42 mrad of lens L_3. The experimental model is, therefore, nearly diffraction limited.

It must be noted that the Gaussian distribution of the pump beam does not degrade the resolution as expected from the physical optics analysis. It can easily be shown that the Gaussian amplitude factor of the angular spectrum of the upconverted image fields becomes unity for all angular frequencies in the image space configuration where the apparent IR object location coincides with the nonlinear material[1].

The primary effect of Gaussian profile of the pump beam appears as intensity reduction of upconverted images toward the edge of FOV. The size of the 10.6-μm image of the object formed at the crystal would, therefore, be considerably smaller than the pump beam size if one wants to avoid intensity reduction at the outer edge of FOV. In the experiment, the size of the 10.6-μm image of the resolution chart at the crystal was 3.6 mm by 3.6 mm (considerably smaller than the pump beam diameter). Loss of brightness and resolution at the edge can even be seen in Figure 4, which was taken with some precaution to minimize the Gaussian window effect. If the pump beam is expanded to 1-inch diameter and usable pump power is increased by four times that of the present system, the number of resolution elements could be increased to a minimum of 130 by 130, since the resolvable image width remains the same.

It was proved experimentally that the [illegible]able image width was unchanged while the magnification of lens L_3 did change.

D. IMAGE SPACE UPCONVERSION WITH A MULTIMODE PUMP BEAM

The purpose of this experiment is to prove that a multimode pump beam can be used in the image space configuration system without sacrificing the resolving power from the single mode pumped image space system. It is widely recognized that the image resolution degrades with an increase of pump beam divergence[2, 4]. This has been demonstrated experimentally for the Fourier space configuration upconverter[1] and for the optical system in which an apparent IR object is located at finite distance from the nonlinear crystal[5, 6, 7].

The reduction of image resolution due to the pump beam divergence (or equivalently the pump beam profile) has been analyzed by the ray tracing technique[2, 4] and the physical optics approach[1]. It has been shown that the amplitude of the angular spectrum of the upconverted image of an on axis point object contains an attenuation factor that depends on the pump beam intensity distribution and the object position[1]. This attenuation factor becomes independent of the pump beam profile when the apparent IR object plane coincides with the equivalent pump beam plane. The resolving power then becomes insensitive to the pump beam profile and will be limited by the thickness aberration. It must be understood, however, that the intensity distribution of the upconverted image depends strongly on the pump

beam intensity distribution. In order to prevent undesirable image intensity variation across the FOV in the image space configuration system, a randomly phased multimode pump beam is preferred over a beam in a single (or a few) higher order modes which may have holes in the beam.

Figure 5 shows reproduced pictures of an upconverted image of the resolution chart. The image shown in Figure 5A was obtained with a TEM_{oo} mode pumped image space system. Figure 5B shows an image obtained with the same system pumped with a multimode beam. The two images remain essentially the same, indicating no degradation of resolution due to the pump beam divergence. It was observed, however, that the image obtained from the multimode pump beam was less bright than that produced by the TEM_{oo} pumped beam. Quantitative comparison of image brightness for these two cases was not carried out.

It appears that dependence of upconversion efficiency upon the pump beam divergence requires further analytical and experimental investigation to design an efficient image upconversion system.

E. IMAGE UPCONVERSION WITH A PULSED PUMP LASER AND A SYNCHRONOUSLY GATED IMAGE TUBE

An experimental model pulse-gated image upconversion system was assembled, and some preliminary experiments were carried out. The optical layout of the model is identical to the image space configuration (Figure 1). A block diagram of electronics circuits used for the synchronous pump pulse generation and gating of the image tube is shown in Figure 6.

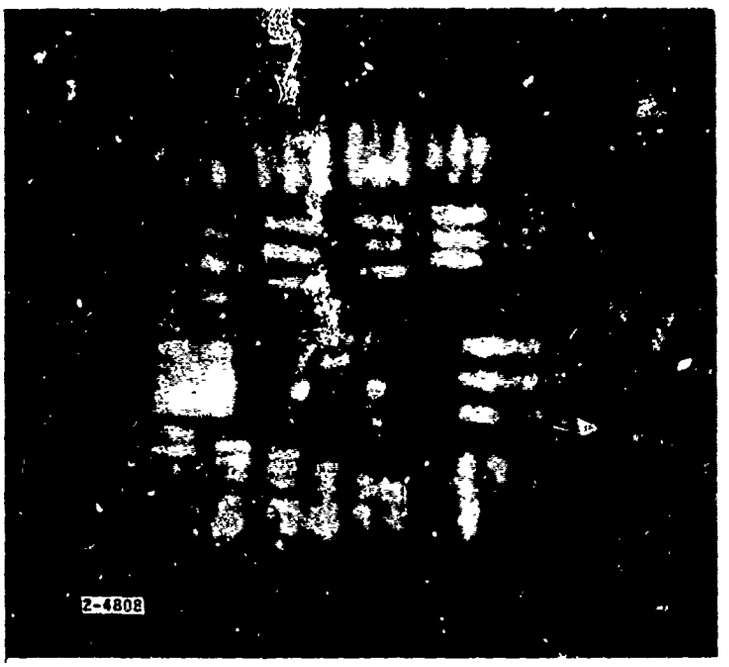

A. TEM_{00} MODE PUMP

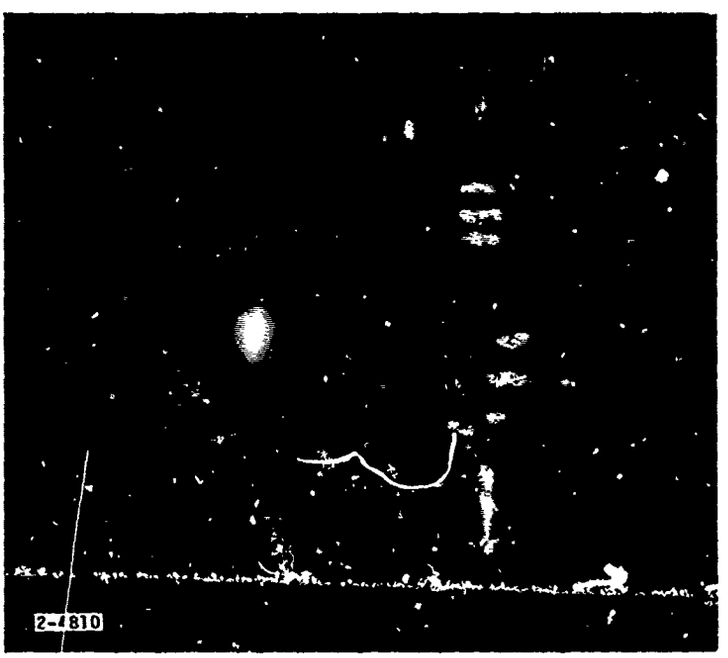

B. MULTIMODE PUMP

FIGURE 5. UPCONVERTED IMAGE OF 1951 USAF TEST CHART PRODUCED BY IMAGE SPACE UPCONVERTER

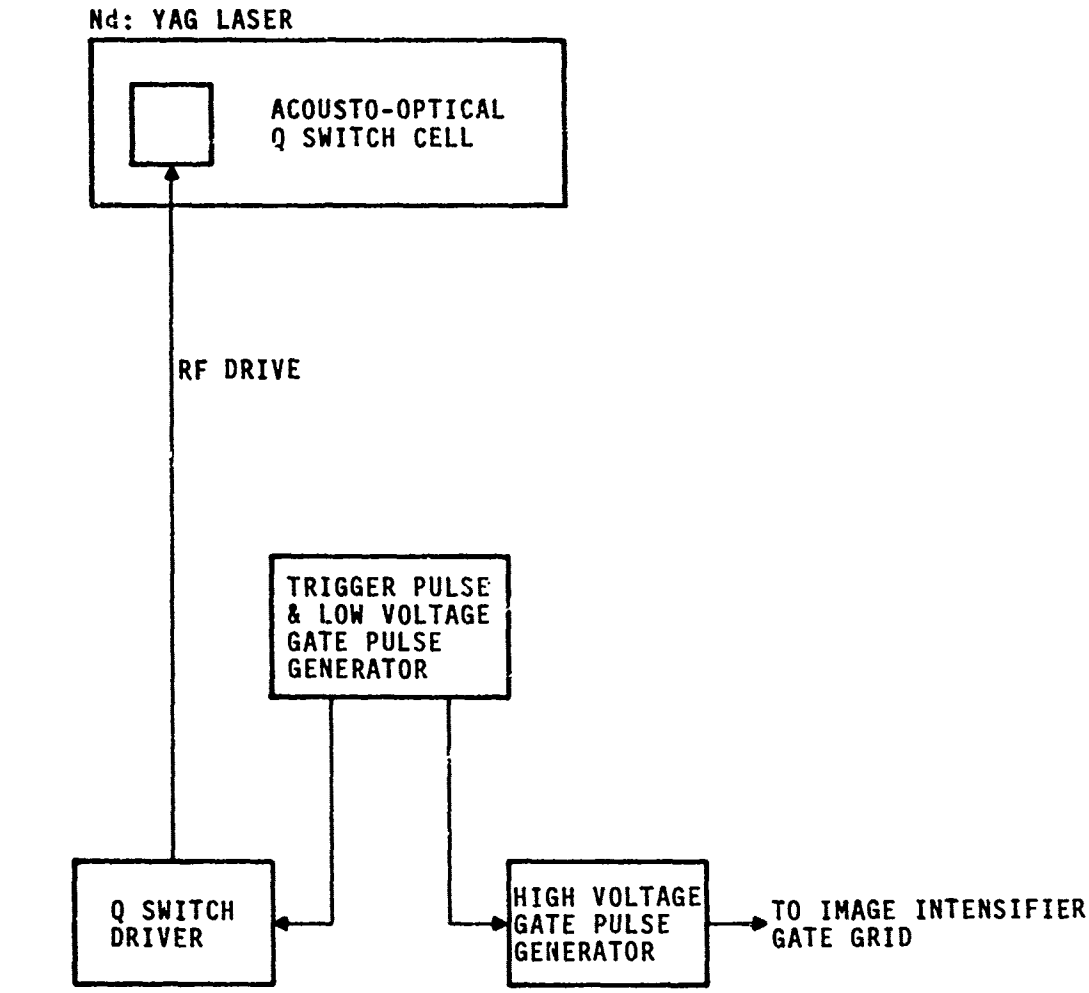

FIGURE 6. BLOCK DIAGRAM OF SYNCHRONOUS GATE ELECTRONICS

The Nd:YAG laser operating in single transverse mode was Q-switched by an acousto-optical Q switch. The pulse repetition rate is controlled by the trigger pulse generator and can be varied from 1 to 5 kHz. Pump pulses with 200-ns duration and approximately 5-kW peak power were expanded to 1-cm diameter. No damage to the crystal was observed. The high voltage gate pulse generator has a 40-ns rise time and an 80-ns fall time. Pulse width and the pulse position of the gate pulses can be adjusted for the optimum image signal-to-noise ratio.

The images obtained with the synchronously gated image tube are shown in Figure 7A. The image shown in Figure 7B is obtained by the same system, but the image tube was not gated. The improvement in the image signal-to-noise ratio attained by gating the image is quite remarkable. Optimization of the experimental system and quantitative measurement of image resolution, conversion efficiency, image SNR, etc., has begun.

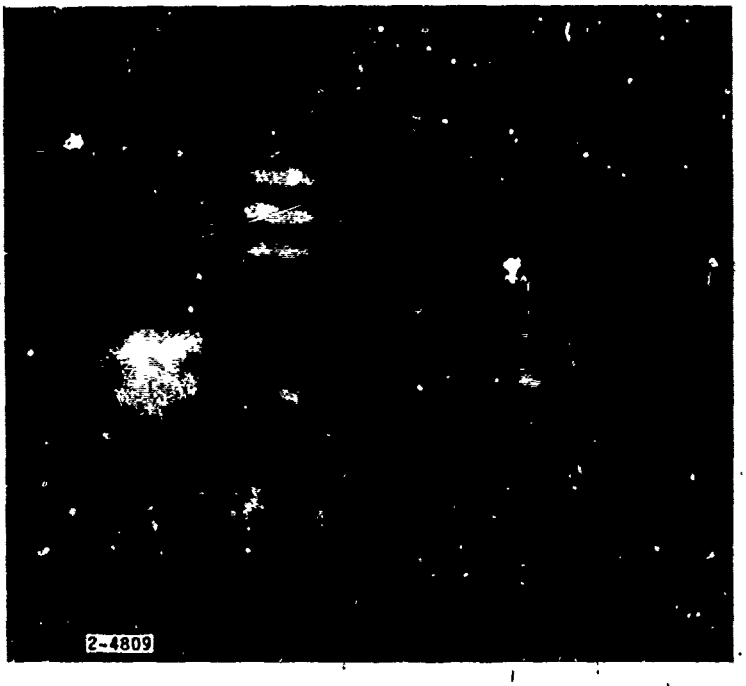

A. SYNCHRONOUSLY GATED IMAGE TUBE

B. UNGATED IMAGE TUBE

FIGURE 7. UPCONVERTED IMAGE WITH A PUMP BEAM

III. ANALYTICAL CONSIDERATIONS

The imaging properties of the parametric image upconversion process have been previously analyzed by the geometric optics (ray tracing) technique[2,4], and the Fourier optics technique [1]. It was shown that the resolving power of the image upconverter is (neglecting the aperture diffraction) limited by thickness aberration and thickness coma. The aberrations are caused by the phase match error inherent in the wide angular spectral of object waves. Analytical expressions for the calculation of abberations, and equations relating the angular spectral of the upconverted image field with object wave Fourier components for different upconverter configurations, were previously reported [2].

It is the purpose of this section to extend previous analysis for further understanding of the parametric image upconversion process. The point spread function and the optical transfer function of a Fourier space configuration upconverter system is discussed first. The result confirms an earlier conclusion of aberration free operation with the Fourier space configuration. Considerations of the resolving power of the image space configuration upconverter systems with plane wave pump are presented next. This treatment follows the geometric optics approach. The effect of material birefringence is considered last. Line spread functions of the plane wave pumped upconverter system are obtained without neglecting the birefringence. Image blurring due to the crystal birefringence could be non-negligible.

A. POINT SPREAD FUNCTIONS AND OPTICAL TRANSFER FUNCTION OF A PLANE WAVE PUMPED INFINITE APERTURE FOURIER CONFIGURATION SYSTEM

Diffraction due to apertures is neglected in this discussion in order to separate image properties of the upconversion process from the diffraction. Lens apertures (the nonlinear material aperture) and the pump beam diameter are, therefore, assumed to be infinitely large.

A simplified schematic of a Fourier space configuration upconverter system is shown in Figure 8. Lens L_1 is positioned such that the object and the front surface of the nonlinear material are respectively in the front and back focal planes. The front local plane of lens L_2 coincide with the exit surface of the nonlinear crystal. Upconverted real image then forms in the back focal plane of lens L_2. Lenses L_1 and L_2 therefore, form a Fourier transform pair. The upconversion takes place in the Fourier transformed space of the object waves; thus the name Fourier space configuration system.

For the plane wave pumped upconverter, it can be shown that the angular spectrum of upconverted image fields in air beyond the nonlinear crystal ($z \geq + D/2$) is related to the Fourier component of object fields over the front surface of the crystal by [1]

$$\mathcal{E}_s(\underline{\kappa}_s, z) \sim \mathcal{E}_i(\underline{\kappa}_s, -D/2)\,\mathrm{Sinc}\left|\frac{\Delta KD}{2}\right| e^{-i\,\Delta KD/2} \quad (1)$$

$$e^{i\left[K_{sz} D + K_{saz}(z - D/2)\right]}$$

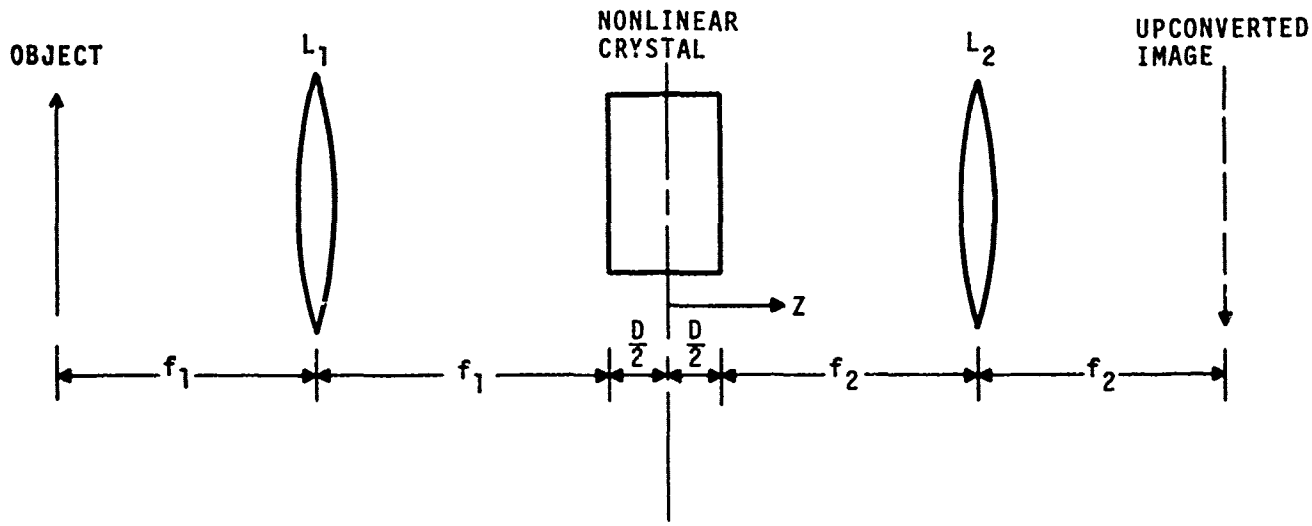

FIGURE 8. IMAGE UPCONVERTER ARRANGED IN FOURIER SPACE CONFIGURATION

where

Sinc x = (sin x)/x

D : material thickness

$K_{sz} = \left(K_s^2 - \underline{\kappa}_s^2\right)^{1/2}$: z component of wave vector at λ_s in the material

K_{saz} : z component of wave vector at λ_s in air

$\Delta K \left(= K_{sz} - K_M - \zeta \kappa_{sx} + \frac{\kappa_s^2}{2K_M}\right)$: phase mismatch factor

K_M : wave vector at λ_s along the phase matched direction

ζ : anisotropy angle

The angular spectrum $\mathcal{E}_i\ (\underline{\kappa}, -D/2)$ is a Fourier transform of the object field distribution over the plane z = -D/2. The object field distribution in the plane z=-D/2 is a Fourier transform of the object field distribution over the front focal plane of lens L_1 since the plane z=-D/2 coincides with the back focal plane of lens L_1 [8].

$$E_i\ (\underline{\rho}, -D/2) = \frac{-i}{\lambda_i} \int E_i\ (\underline{\rho}_i, -2f_1 - D/2)\ e^{-i \frac{K_{ia}}{f_1} \left(\underline{\rho} \cdot \underline{\rho}_i\right)}\ d\underline{\rho}_i \quad (2)$$

and

$$\mathcal{E}_i\ (\underline{\kappa}, -D/2) = \frac{1}{(2\pi)^2} \int E_i\ (\underline{\rho}, -D/2)\ e^{-i\, \underline{\kappa} \cdot \underline{\rho}}\ d\underline{\rho} \quad (3)$$

where

f_1 = focal length of lens L_1

$\underline{\rho}_i$ = transverse position in the front focal plane of lens L_1

$\underline{\rho}$ = transverse position in the back focal plane ($z = -D/2$) of lens L_1

Substituting Equation (2) into Equation (3) and carrying out the integration we obtain

$$\mathcal{E}_i(\underline{\kappa}, -D/2) \sim E_i(-f_1/K_{ia}, -2f_1 - D/2) \qquad (4)$$

Constant Amplitude factor and fixed phase factors have been omitted in Equation (4) since they do not affect the result in any significant way. Equation (4) indicates that the angular spectrum of field distribution over the back focal plane of a nondiffracting thin lens has the same functional form as the field distribution over the front focal plane of the lens. This result is no surprise if one realizes that they are related by double Fourier transform.

The field distribution of an upconverted image formed in the back focal plane of lens L_2 has the same functional form as $\mathcal{E}_s(\underline{\kappa}_s, -D/2)$ since the plane $z = +D/2$ and the upconverted image plane are two focal planes of lens L_2.

$$\bar{E}_s\,(\underline{\rho}_s,\ 2f_2 + D/2) \sim \mathcal{E}_s\,(K_{sa}\,\rho_s / f_2\ ,\ D/2) \qquad (5)$$

Combining Equations (1), (4), and (5), we obtain an expression for the upconverted image field distribution

$$E_s\,(\underline{\rho}_s,\ 2f_2 + D/2) \sim E_i\,(-\frac{K_{sa}\,f_1}{K_{ia}\,f_2}\,\underline{\rho}_i,\ -2f_1 - D/2). \qquad (6)$$

$$\mathrm{Sinc}\,(\frac{\Delta KD}{2})\,e^{-i\left(\frac{\Delta KD}{2} - K_{sz}D\right)}$$

where mismatch factor ΔK and the z component wave vector K_{sz} in Equation (6) are evaluated by replacing $\underline{\kappa}_s$ with $K_{sa}\,\underline{\rho}_s/f_2$ and are given by

$$\Delta K = K_s - K_M - \zeta\,K_{sa}\,x_s/f_2 + \frac{K_{sa}^{\,2}}{2f_2^{\,2}}\,\rho_s^{\,2}\ \left(\frac{1}{K_M} - \frac{1}{K_s}\right) \qquad (7)$$

and

$$K_{sz}^{\,2} = K_s^{\,2} - (K_{sa}\,\rho/f_2)^{\,2} \qquad (8)$$

If crystal anisotropy is neglected the mismatch factor ΔK is

$$\Delta K = -\frac{K_p}{2K_M K_i}\left(\frac{K_{sa}}{f_2}\ \rho_s\right)^2 \qquad (9)$$

The function $\mathrm{sinc}\left[\frac{K_p D}{4K_M K_i}\left(\frac{K_{sa}}{f_2}\,\rho_s\right)^2\right]$ indicates that the amplitude of an upconverted image field of a uniformly illuminated object field will not be uniform but will decrease with transverse distance ρ_s. It imposes a limitation on the size of the upconverted image but will not limit the image

resolution. If we define the size of an upconverted image as equal to the transverse distance ρ_s, where the first zero of a sinc x function occurs, the radius of an upconverted image is expressed by

$$a_s = 2\frac{f_2}{K_{sa}}\sqrt{\frac{\pi K_M K_i}{D K_p}} \tag{10}$$

Equation (6) also shows that the transverse magnification of a Fourier space configuration upconverter system is

$$M_t = -\frac{K_{ia} f_2}{K_{sa} f_1} = -\frac{\lambda_s f_2}{\lambda_i f_1} \tag{11}$$

Equation (11) can also be obtained by the geometric optics analysis. The limiting size of an object that can be upconverted can be easily found by combining Equations (10) and (11).

$$a_i = a_s / |M_t| = 2\frac{f_1}{K_{ia}}\sqrt{\frac{\pi K_M K_i}{D K_p}} \tag{12}$$

Noting that the object size a_i is related to the acceptance angle θ_{ia} (FOV) of the upconverter by

$$2a_i = f_1 \theta_{ia}$$

we obtain

$$\theta_{ia} = 2\left(\frac{2\lambda_p \lambda_i n_i n_{sM}}{\lambda_s n_p D}\right)^{1/2} \tag{13}$$

For a noncritically phased matched proustite unconversion from 10.6 μm to 0.967 μm, we have $\theta_{ia} = 0.157 \left(\frac{1}{D} \right)^{1/2}$ rad.

To illustrate the points presented in the previous discussion let us consider a case where the object field distribution is a sine function as shown in Figure 9A. The field distribution of upconverted image formed in the back focal plane of lens L_2 is shown in Figure 9B. The period of the sine function image field is magnified by a factor M_t and its amplitude envelope follows the sinc function. The image is inverted as shown in Figure 9B so that an object point $-y_{i1}$ is imaged at $y_{s1} = -M_t\, y_{i1}$. The resolving power is unlimited since the image field period is linearly proportional to the object field period. The object size that can be upconverted is, however, limited. The size limitation is caused by the phase match requirement rather than the crystal aperture limitation.

The point spread function, which is a response to a point object, is easily obtained from Equation (6). The field distribution of a point object at (x_{io}, y_{io}) is expressed

$$E_i\,(\underline{\rho}_i) \sim \delta\,(x_i - x_{io}) \cdot \delta(y_i - y_{io})$$

Then from Equation (6), the point spread function becomes

$$H_s\,(\underline{\rho}_s) \sim \delta\,(x_s/M_t - x_{io})\,\delta(y_s/M_t - y_{io}) \left[\mathrm{Sinc}\left(\frac{\Delta K D}{2}\right) \cdot e^{-i\,(\Delta K/2 - K_{sz})\,D} \right]_{\underline{\kappa} = K_{sa} M_t \rho_{io}/f_2} \quad (14)$$

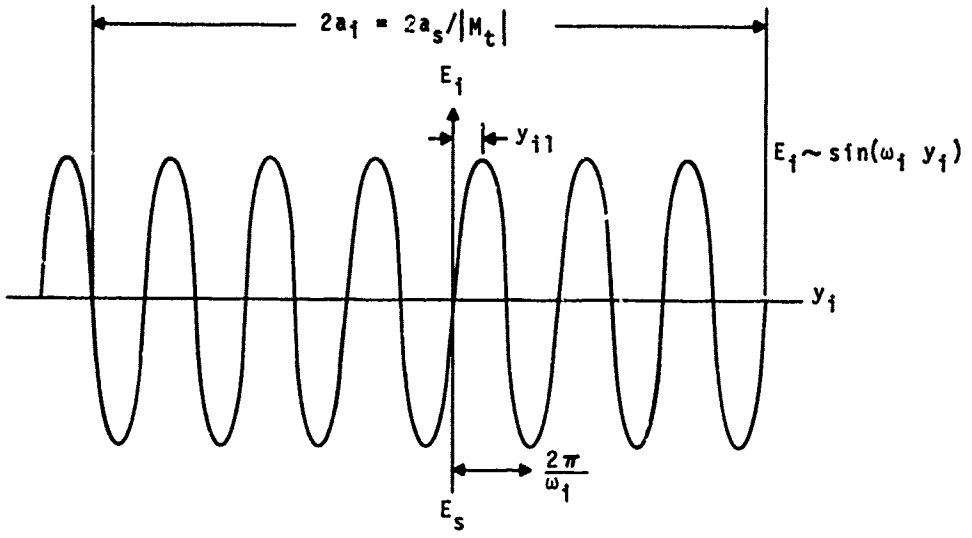

A. OBJECT FIELD DISTRIBUTION

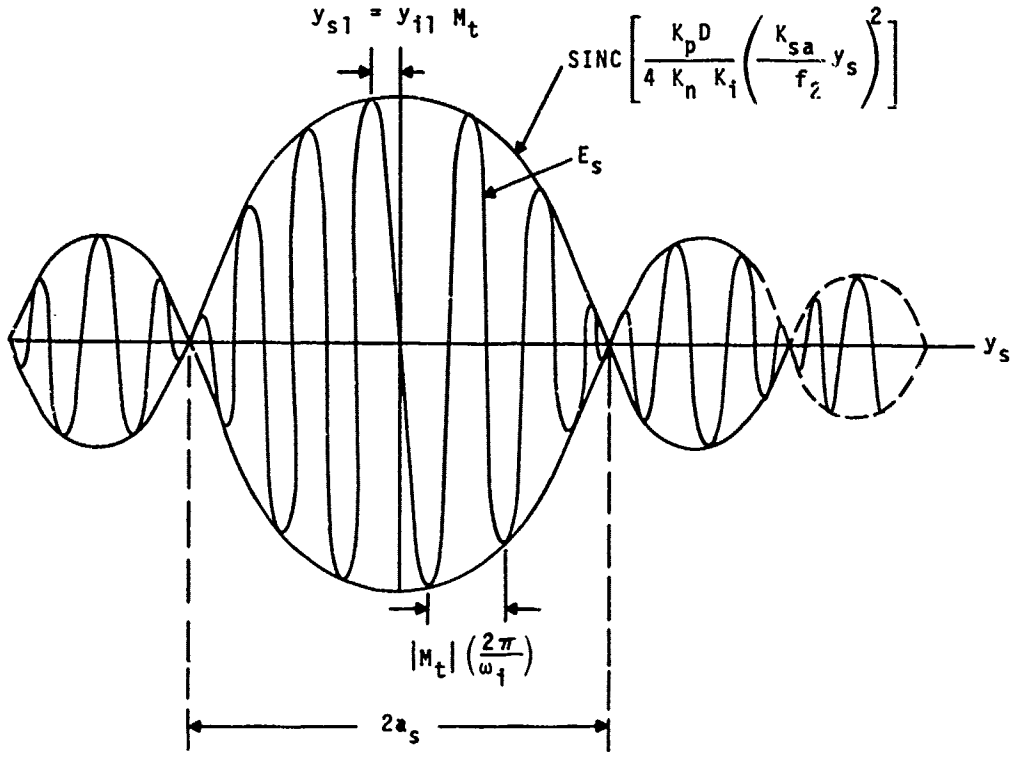

B. UPCONVERTED IMAGE FIELD DISTRIBUTION

2-4815

FIGURE 9. FIELD DISTRIBUTION OF OBJECT AND UPCONVERTED IMAGE FOR THE FOURIER SPACE CONFIGURATION

where $\left[\quad\right]_{\underline{\kappa} = K_{sa}\underline{\rho}_s / f_2}$ indicates that the quantity inside the bracket is evaluated at $\underline{\kappa} = K_{sa}\underline{\rho}_s/f_2$ as shown in Equation (7) and Equation (8).

The coherent transfer function, which is the Fourier transform of the point spread function, becomes

$$h_s(\underline{\kappa}_s) \sim M_t^2 \, e^{-i M_t \underline{\kappa}_s \cdot \underline{\rho}_{io}} \left[\mathrm{Sinc}\left(\frac{\Delta K D}{2}\right) \cdot e^{-i\left(\frac{\Delta K}{2} - K_{sz}\right) D} \right]_{\underline{\kappa} = K_{sa} M_t \underline{\rho}_{io} / f_2} \tag{15}$$

Amplitude of $h_s(\underline{\kappa}_s)$ depends on the object location and thus object size limitation is implied even for the infinite aperture Fourier configuration upconverter. The optical transfer function, which is defined [8] as,

$$\mathcal{H}_s(\underline{\kappa}) = \frac{\iint h_s(\underline{\kappa}') \cdot h_s^*(\underline{\kappa}' + \underline{\kappa}) \, d\underline{\kappa}'}{\iint h_s(\underline{\kappa}')^2 \, d\underline{\kappa}'} \tag{16}$$

becomes

$$\mathcal{H}_s(\underline{\kappa}) = e^{i M_t \underline{\kappa} \cdot \underline{\rho}_{io}} \tag{17}$$

Equation (17) again indicates the property of unlimited resolving power since the amplitude of optical transfer function (Modulation transfer function) is independent of angular frequency $\underline{\kappa}$.

B. RESOLVING POWER OF THE IMAGE UPCONVERTER IN NON-FOURIER SPACE CONFIGURATION

Resolving power of the plane wave pumped image upconverter systems is considered in these paragraphs. The crystal birefringence is neglected and paraxial assumption is used. Computational procedure based on the ray tracing approach has been suggested previously without detailed discussions [2]. The present consideration is intended to give computational formulas for various optical arrangements.

It has been shown, both from the geometric optics [2] and the physical optics considerations [1], that the minimum resolvable image width of the non-Fourier space configuration is independent of the longitudinal object location if the thickness aberration is the only factor affecting image resolution. It has also been shown that transverse magnification of the plane wave pumped upconverter is independent of object location and is equal to the resolvable upconverted image width.

Resolution of two types of non-Fourier space configuration is considered based on the geometric optics approach. Two optical systems, following Andrew's designation, are schematically shown in Figure 10. The optical system II (Figure 10A) has the following arrangement.

A real object is located a distance S from the nonlinear material and no intervening image forming components such as lenses and mirrors exist between the object and the nonlinear material. The upconverter aperture is limited by either the crystal size or the pump beam size. The

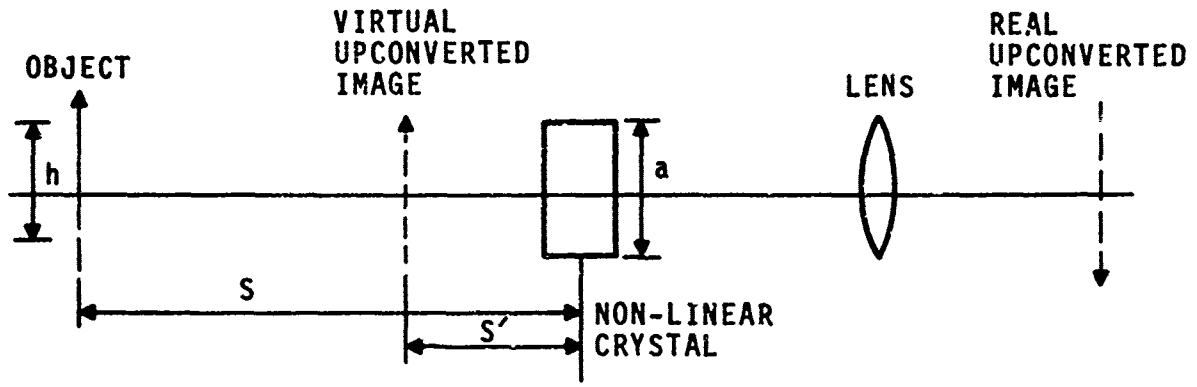

A. OPTICAL SYSTEM II

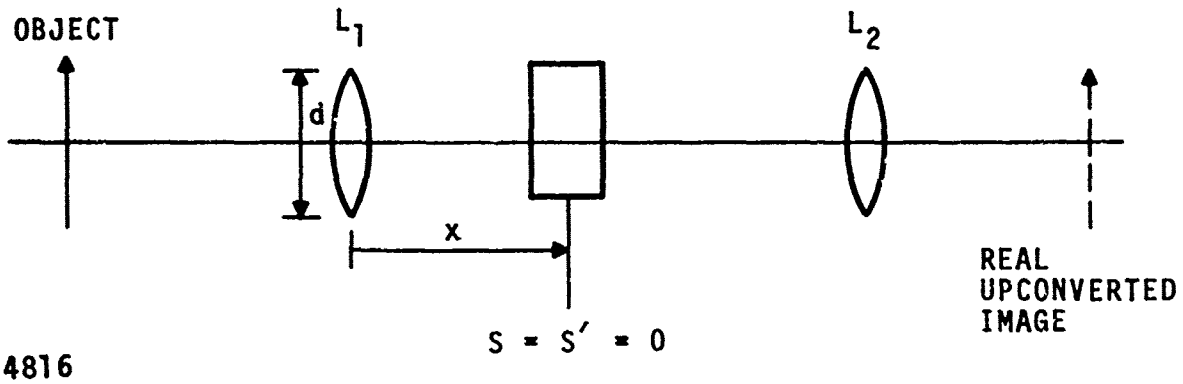

2-4816

B. OPTICAL SYSTEM I

FIGURE 10. IMAGE UPCONVERTER SYSTEMS OF NON-FOURIER SPACE CONFIGURATION

FOV of the system is equal to the upconverter acceptance angle θ_{ia} and the object size H is limited to

$$H = S \tan \theta_{ia} \tag{18}$$

From the geometry

$$\tan \theta_{imax} = (h + a)/2S \tag{19}$$

Since object rays entering the crystal with the incidence angle larger than one half of acceptance angle will not be effectively upconverted, the upper limit of θ_{imax} is one half of acceptance angle.

According to the geometric optics analysis, the resolvable transverse image width of a plane wave pumped image upconverter operating in the non-Fourier space configuration is expressed by [2]

$$\Delta h = D \left(\frac{1 - \beta}{n_i} \right) \tan \theta_{imax} \tag{20}$$

where

D = material thickness

$\beta (= K_i/K_s = n_i \lambda_s / n_s \lambda_i)$ = Angular demagnification factor

n_i = Index of refraction at n_i along the phase match direction

θ_{imax} = Angle between the extreme object rays and the reference axis.

The angular resolution γ can be calculated using Equations (19) and (20)

$$\gamma = \tan^{-1} (\Delta h/S) = \tan^{-1} \left[D (1-\beta) (h + a)/2 n_i S^2 \right] \tag{21}$$

Equation (21) indicates that resolution at the extremities of the image is poorer than that at the center. The angular resolution at the extremities and at the center of the image are respectively

$$(\gamma)_{\text{center}} = \tan^{-1}\left[\text{Da}\,(1-\beta)/2\,n_i\,S^2\right] \qquad (22)$$

$$(\gamma)_{\text{extreme}} = \tan^{-1}\left[D\,\theta_{ia}\,(1-\beta)/2\,n_i S\right] \qquad (23)$$

It must be remembered that equations (22) and (23) hold only for the paraxial system ($S > a$). The minimum resolvable angle cannot be smaller than the Rayleigh resolution angle of the limiting aperture. If the crystal aperture is the limiting aperture it is

$$\gamma_{min} = 1.22\,\lambda_i/a$$

The number of resolution elements contained in the FOV is then

$$R = \theta_{ia}/\gamma$$

The upper and the lower bound of the number of resolution elements for the paraxial system are:

$$\frac{a\,\theta_{ia}}{1.22\,\lambda_i} \geq R = \frac{2\,n_i\,S^2\,\theta_{ia}}{\text{Da}\,(1-\beta)} \geq \frac{2\,n_i\,S}{D\,(1-\beta)} \qquad (24)$$

In the optical system I, an objective lens is used to form an IR image of objects in the central plane of nonlinear crystal (Figure 10B). Under the paraxial assumption the extreme angle θ_{imax} is equal to half the angle subtended by the objective lens at the nonlinear crystal

$$\theta_{imax} = d/2\,x \leq \theta_{ia}/2 \qquad (25)$$

d = effective object lens diameter
x = distance between the object lens and the crystal

Again θ_{imax} is bounded by the half acceptance angle. The minimum resolvable image size is

$$\Delta h' = D\,(1-\beta)\,d/2_x n_i \leq D\,(1-\beta)\,\theta_{ia}/2\,n_i \qquad (26)$$

The maximum number of linear resolution elements is

$$R = a/\Delta h' = \frac{2ax\,n_i}{D\,(1-\beta)\,d} = \frac{2\,a\,n_i}{D\,(1-\beta)\,\theta_{ia}} \qquad (27)$$

For the system imaging distant objects the distance x is equal to the focal length f_1 of lens L_1 and the ratio x/d can be replaced by the F number of lens L_1. The upper bound of resolving power is again limited by the lens aperture diffraction.

$$1.22\,\lambda_i F_1 > R = \frac{2a\,n_i}{D\,(1-\beta)}\quad F_1 > \frac{2a\,n_i}{D\,(1-\beta)\,\theta_{ia}} \qquad (28)$$

Combining equation (13) and the right hand side of equation (28) the lower bound of the object lens F number for the distant object imaging system is,

$$F_1 \geq \left(\frac{\lambda_s\,n_p\,D}{8\,\lambda_p\,\lambda_i\,n_i\,n_{sm}}\right)^{1/2} \qquad (29)$$

The angular resolution of the optical system I for upconversion of distant objects is

$$\gamma = \Delta h/f_1 = D\,(1-\beta)\,/2n_i\,F_1 f_1 \leq D\,(1-\beta)\,\theta_{ia}/2\,n_i\,f_1 \qquad (30)$$

The worst angular resolution is obtained when the F number of the object lens is equal to the lower bound; that is, $F_1 = 1/\theta_{ia}$.

The diffraction limited resolution may be obtained when the F number of the object lens is

$$F_1 = \left[\frac{D\,(1-\beta)}{2.44\,\lambda_i\,n_i} \right]^{1/2} \qquad (31)$$

C. EFFECTS OF CRYSTAL BIREFRINGENCE

In this paragraph we will consider effects of the crystal birefringence upon imaging properties of the upconverter. Negligible aperture diffraction and plane wave pump are assumed in order to isolate the birefringent effect from others. The Fourier optics formalism used in paragraph A is adopted.

1. IMAGE SPACE CONFIGURATION

Omitting constant amplitude and phase factors, the angular spectrum of upconverted field emanating out of the crystal back surface is[1]

$$\mathcal{E}_s(\underline{\kappa}, z) \sim \mathcal{E}_i(\underline{\kappa}, -s)\,\mathrm{Sinc}\left[\frac{D}{2}\left(\frac{\kappa^2 K_p}{2K_M K_i} + \zeta\kappa_x\right)\right] \cdot \qquad (32)$$

$$e^{i\left[\frac{\zeta D}{2}\kappa_x - \Phi\left(\kappa^2, z\right)\right]}$$

where

$$\Phi(\kappa^2, z) = \frac{\kappa^2}{2}\left(\frac{z - D/Z}{K_{sa}} + \frac{S - D/2}{K_{ia}} + \frac{D}{2K_M} + \frac{D}{2K_s}\right) \qquad (33)$$

The electric field distribution in the upconverted image field becomes

$$E_s(\underline{\rho}_s, z) \sim \int d\underline{\kappa}\ \mathcal{E}_i(\underline{\kappa}, -s)\ \mathrm{Sinc}\left(\frac{\Delta KD}{2}\right) \cdot \qquad (34)$$

$$e^{-i\left[\Phi(\kappa^2, z) - \kappa_x(x_s - \zeta D/2) + \kappa_y y_s\right]}$$

Equation (34) indicates that the optimum focusing condition is

$$\Phi(\kappa^2, z) \equiv 0 \quad \text{for all } \kappa$$

The solution, which defines the upconverted image plane,

$$z = -S' = -\frac{K_{ia}}{K_{sa}}\ S - \frac{DK_{sa}}{2}\left[\frac{1}{K_M} + \frac{1}{K_s} - \frac{1}{K_{ia}} - \frac{1}{K_{sa}}\right] \qquad (35)$$

is identical to the case of negligible birefringence system and defines the image plane.

The line spread function of a line object parallel to the x axis will be considered first. The object field distribution and its angular spectrum are

$$E_i(\underline{\rho}_i, -s) \sim \delta(y - y_{io})$$

$$\mathcal{E}_i(\underline{\kappa}, -s) \sim e^{-i\kappa_y y_{io}}\,\delta(\kappa_x) \qquad (36)$$

The line spread function is then

$$E_s(x_s, y_s, -S') \sim \int \mathrm{Sinc}\left(\frac{DK_p}{4K_M K_i}\ \kappa_y^2\right) e^{+i\kappa_y(y_s - y_{io})}\, d\kappa_y$$

Evaluating the integration, we obtain

$$E_s(x_s, y_s - y_{io}, -S') \sim \frac{4\pi K_M K_i}{K_p D} (y_s - y_{io}) \left[S\left(\sqrt{\frac{2K_M K_i}{\pi K_p D}} (y_s - y_{io}) \right) \right.$$

$$\left. -C \left(\sqrt{\frac{2K_M K_i}{\pi K_p D}} (y_s - y_{io}) \right) \right] + 4 \sqrt{\frac{\pi K_M K_i}{K_p D}} \operatorname{Sin} \left[\frac{K_M K_i}{K_p D} (y_s - y_{io})^2 + \frac{\pi}{4} \right] \tag{37}$$

where Fresnel functions S(X) and C(y) are defined

$$S(X) = \int_0^X \sin \left(\frac{\pi}{2} t^2 \right) dt$$

$$C(X) = \int_0^X \cos \left(\frac{\pi}{2} t^2 \right) dt$$

The expression (37) applies equally to the system with negligible birefringence. This result indicates that the image quality is not degraded along the y direction which is normal to the plane containing optic axis C and the z axis (Figure 11). The line spread function is only a function of normal distance $(y_s - y_{io})$.

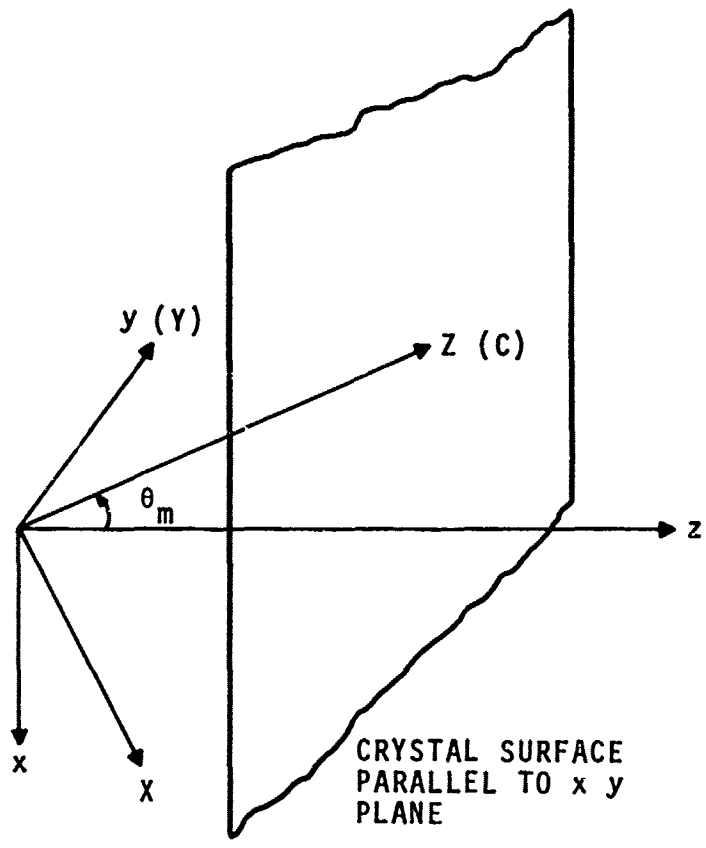

2-4817

FIGURE 11. RELATION BETWEEN THE COORDINATES (x, y, z) AND THE CRYSTALLOGRAPHIC AXIS (X, Y, Z)

The line spread function of a line object parallel to the y axis is considered next. The object field distribution and its angular spectrum are

$$E_i(\underline{\rho}_i, -S) \sim \delta(x_i - x_{io})$$

$$\mathcal{E}_i(\underline{\kappa}, -S)\ e^{-i\kappa_x x_{io}}\ \delta(\kappa_y)$$

The line spread function is

$$E_s(x_s - x_{io} - \frac{\zeta D}{2},\ y_s,\ -S') \sim \int d\kappa_x\ \mathrm{Sinc}\left[\frac{D}{2}\left(\frac{\kappa_x 2K_p}{2K_M K_i} + \zeta\kappa_x\right)\right] \cdot e^{i\kappa_x\left(x_s - x_{io} - \frac{\zeta D}{2}\right)} \tag{38}$$

Rewriting above equation,

$$E_s(x_s' - x_{io},\ y_s,\ -S') \sim e^{-i\frac{\zeta K_M K_i}{2K_p}x'} \int d\kappa\ \mathrm{Sinc}\left\{\frac{K_p D}{4K_M K_i}\left[\kappa^2 - \left(\frac{\zeta K_M K_i}{K_p}\right)^2\right]\right\} \cdot e^{i\kappa(x_s' - x_{io})} \tag{39}$$

where

$$x_s' = x_s - \frac{\zeta D}{2}$$

Equation (39) indicates that crystal birefringence affects the upconverted image in following ways:

- Introducing change in the field distribution from that of non-birefringent case

- The field distribution is a function of $(x_s - x_{io} - \zeta D/2)$ rather than $x_s - x_{io}$. This implies that the x coordinate of upconverted image is translated toward positive x direction by an amount $\zeta D/2$, (Figure 12). This linear translation becomes obvious if one realizes that energy flow inside the material is along the anisotropy direction rather than along the z direction.

Line spread functions along two orthogonal directions expressed by equation (37) and equation (39) are evaluated for a 1.06-μm pumped 1 cm long proustite crystal upconverting 10.6-μm objects into 0.967-μm images. The results are plotted in Figure 13. The amplitude of the spread functions is normalized to the peak amplitude of the line spread function parallel to the x axis.

Resolvable image line width along the y direction can be determined by Rayleigh criterion since the sidelobes of the spread function parallel to the x axis are considerably lower compared to the mainlobe.

The spread function parallel to the y axis contains several nearly equal amplitude lobes as seen in Figure 13. The amplitude of these lobes is considerably lower than that of the mainlobe of the x direction line spread function. The width of these lobes is also narrower than that of the x direction line spread function. Rayleigh resolution criterion cannot be used to determine resolution along the x direction, because the adjacent lobes are nearly equal in amplitude.

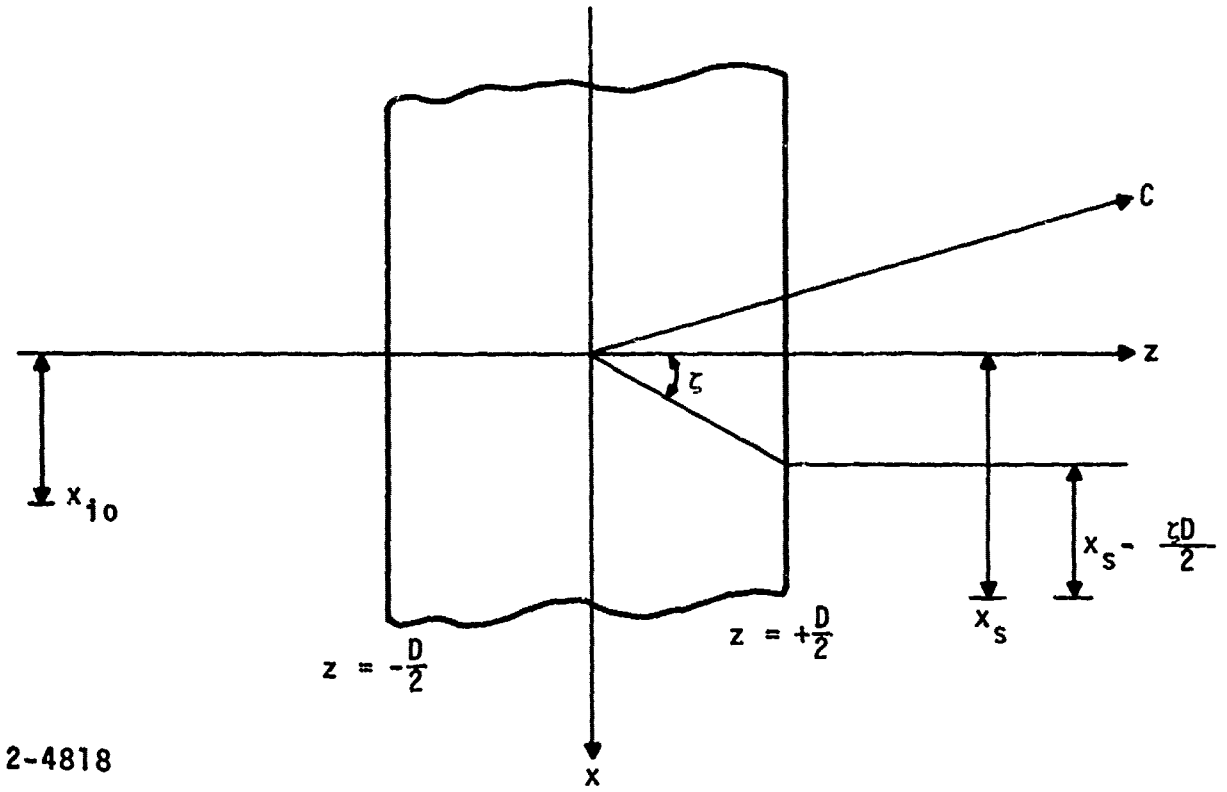

FIGURE 12. GEOMETRIC RELATIONSHIP BETWEEN X COORDINATE OF IR OBJECT FIELD AND X COORDINATE OF UPCONVERTED IMAGE FIELD

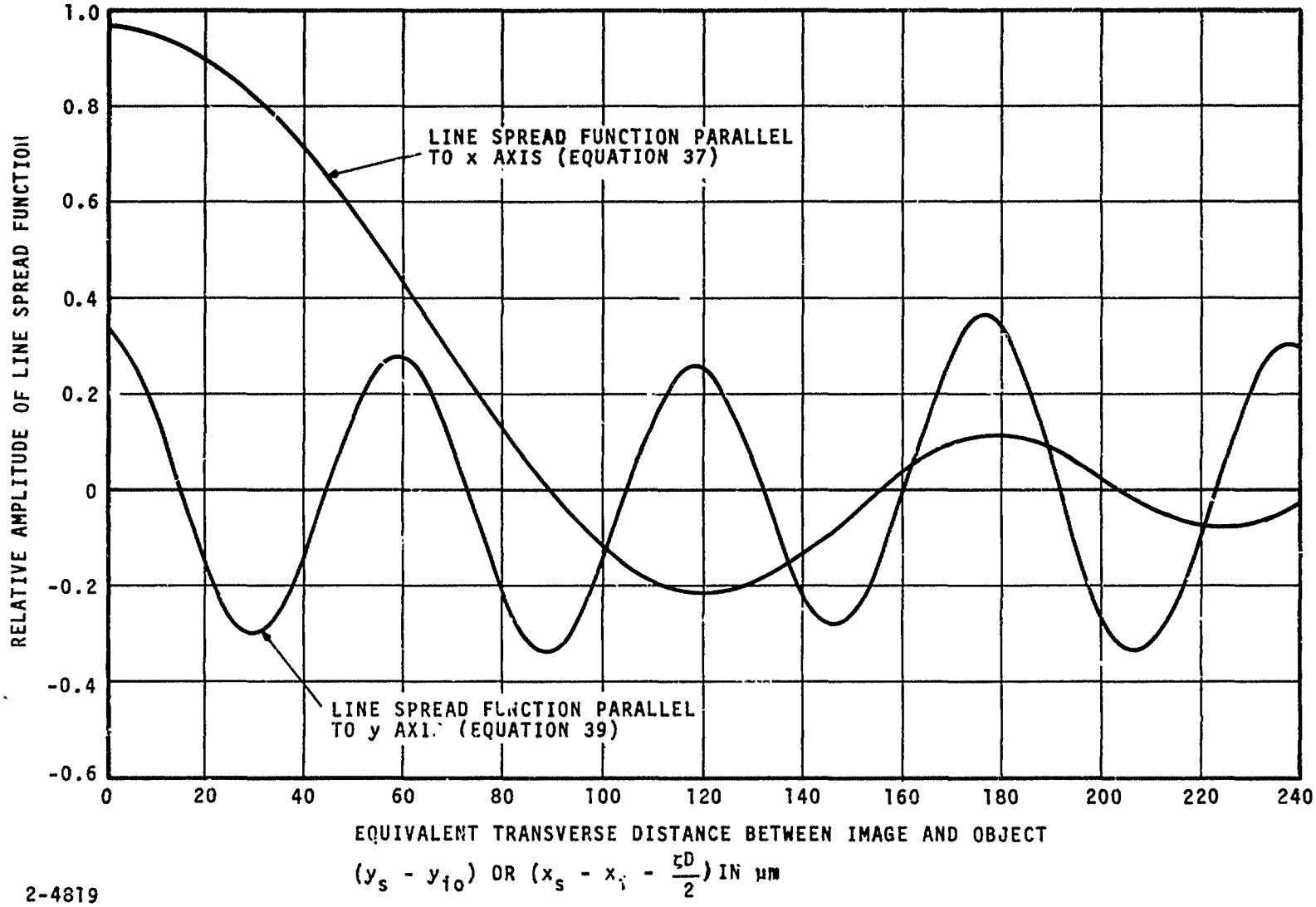

FIGURE 13. RELATIVE AMPLITUDE OF LINE SPREAD FUNCTIONS FOR 1 cm LONG PROUSTITE

Resolution degradation along the x axis predicted from Figure 12 has not been observed in the experiments described in paragraph C of Section II. One of possible causes for not observing resolution degradation is due to the masking of birefringent effect by relatively larger diffraction line width of the object lens.

More careful measurements of line spread function parallel to the y axis are necessary in order to observe the effect of crystal birefringence.

2. FOURIER SPACE CONFIGURATION

It has been shown in paragraph A that the field distribution of upconverted image formed in the back focal plane of lens L_2 (Figure 8) is related to the object field distribution over the front focal plane of lens L_1 by repeating equations (6), (7), and (8)

$$E_s(\underline{\rho}_s) \sim E_i\left(\frac{-K_{sa} f_1}{K_{ia} f_2}\ \underline{\rho}_s\right)\ \text{Sinc}\left(\frac{\Delta K D}{2}\right)\ e^{-i\left(\frac{\Delta K D}{2} - K_{sz} D\right)} \tag{6}$$

where ΔK and K_{sz} are given by equations (7), and (8)

$$\Delta K = -\frac{K_p}{2K_M K_i}\left(\frac{K_{sa}}{f_2}\ \underline{\rho}_s\right)^2 - \zeta \frac{K_{sa}}{f_2} x_s \tag{7}$$

$$K_{sz} = K_s^2 - \left(\frac{K_{sa}}{f_2}\ \underline{\rho}_s\right)^2 \tag{8}$$

From previous equations we can conclude:

- Magnification along two orthogonal transverse directions is not affected by the crystal birefringence. This implies no distortion.
- Different amplitude envelope along two orthogonal transverse axes. This implies different acceptance angle for two directions. Acceptance angle in the yz plane is given by equation (13). In the xz plane it becomes:

$$\theta_{iax} = 2\frac{\lambda_p n_s}{\lambda_s n_p}\left[\left(\zeta^2 + \frac{2n_p\lambda_s\lambda_i}{\lambda_p n_x n_i}\right)^{1/2} - \zeta\right] \qquad (40)$$

- No degradation in resolving power, since the factor $\text{Sinc}\left(\frac{\Delta KD}{2}\right)$ in equation (6) only affects the envelope of image.

D. POINT SPREAD FUNCTION OF A GAUSSIAN BEAM PUMPED FOURIER SPACE CONFIGURATION SYSTEM

The effect of pump beam amplitude distribution on the imaging characteristics of the Fourier space configuration image upconverter is considered. Diffraction due to the lens apertures and the crystal birefringence are neglected. It is also assumed that the physical size of the nonlinear material is large compared to the pump beam size. The optical arrangement is shown in Figure 8.

The pump beam is assumed to be in the TEM_{oo} mode. The Gaussian window at the entrance surface of the nonlinear crystal is expressed by*

$$E_p(\underline{\rho}, -D/2) \sim e^{-\underline{\rho}^2/a^2} \tag{42}$$

The angular spectrum of pump field distribution is

$$\mathcal{E}_p(\underline{\kappa}_p, -D/2) \sim e^{-a^2 \underline{\kappa}_p^2/4} \tag{43}$$

The point object in the front focal plane of the object lens is expressed by

$$E_i(\underline{\rho}_i, -2f_1 - D/2) \sim \delta(\underline{\rho}_i - \underline{\rho}_{io}) \tag{44}$$

The angular spectrum in the IR object fields in the entrance plane of the crystal is, using equation (4),

$$\mathcal{E}_i(\underline{\kappa}_i, -D/2) \sim E_i(-f_1 \underline{\kappa}_i/K_{ia}, -2f_1 - D/2) \sim \delta(\underline{\kappa}_i + K_{ia}\underline{\rho}_{io}/f_1) \tag{45}$$

The sum-frequency polarization P_s is obtained by taking a convolution of $\mathcal{E}_i(\underline{\kappa}_i, -D/2)$ and $\mathcal{E}_p(\underline{\kappa}_p, -D/2)$.

---

*Constant amplitude and phase factors are again omitted in the following analysis.

$$P_s(\underline{\kappa}_s, -D/2) \sim \int \mathcal{E}_i(\underline{\kappa}_i, -D/2)\, \mathcal{E}_p^*(\kappa_s - \underline{\kappa}_p, -D/2)\, d\underline{\kappa}_i$$

$$\sim e^{-a^2(\underline{\kappa}_s + K_{ia}\underline{\rho}_{io}/f_1)^2/4} \tag{46}$$

The angular spectrum of upconverted image fields at the exit surface of the crystal is

$$\mathcal{E}_s(\underline{\kappa}_s, +D/2) \sim e^{-a^2(\underline{\kappa}_s + K_{ia}\underline{\rho}_{io}/f_1)^2/4}\ \mathrm{Sinc}\left(\frac{\Delta K D}{2}\right) e^{-iD\left(K_{sz} + \frac{\Delta K}{2}\right)} \tag{47}$$

where ΔK and K_{sz} are mismatch factors and the z component of wave vector in the material for the angular spectrum with the angular frequency $\underline{\kappa}_s$.

Field distribution of the upconverted image in the back focal plane of the imaging lens is, by equation (5)

$$E_s(\underline{\rho}_s, 2f_2 + D/2) \sim \mathcal{E}_s(K_{sa}\underline{\rho}_s/f_2, +D/2)$$

$$\sim e^{-a^2\left(\frac{K_{sa}}{f_2}\underline{\rho}_s + \frac{K_{ia}}{f_1}\underline{\rho}_{io}\right)^2/4} \left[\mathrm{Sinc}\left(\frac{\Delta K D}{2}\right) e^{-iD(K_{sz} + \Delta K/2)}\right]_{\underline{\kappa}_s = \frac{K_{sa}}{f_2}\underline{\rho}_s} \tag{48}$$

The symbol $\left[\quad\right]_{\underline{\kappa}_s = \frac{K_{sa}}{f_2}\underline{\rho}_s}$ indicates again that ΔK and K_{sz} are evaluated by replacing $\underline{\kappa}_s$ with $K_{sa}\,\underline{\rho}_s/f_2$ as shown in equations (7) and (8).

Equation (48) is the point spread function of Gaussian beam pumped Fourier space configuration image upconverter. The upconverted image is no longer a point. The sinc function again limits the FOV of the system and describes the amplitude envelope of the image plane in the similar way as the plane wave pumped case. The Gaussian amplitude factor

$$e^{-\left(\frac{a K_{ia}}{2 f_1}\right)^2 \left(\frac{f_1 K_{sa}}{f_2 K_{ia}}\underline{\rho}_s + \underline{\rho}_{io}\right)^2}$$

indicates that transverse magnification factor M_t and the image spot size are given by

$$M_t = \underline{\rho}_s \Big/ \underline{\rho}_i = -f_2 K_{ia} \Big/ f_1 K_{sa} \tag{49}$$

$$W_s = 2 f_2 \Big/ a K_{sa} \tag{50}$$

Equation (49) is identical to equation (11). It implies that the Gaussian amplitude distribution does not introduce distortion. Combining equations (49) and (50) and dividing the object spot size by the focal length of the object lens we obtain expressions for the resolvable IR object spot size and angle;

$$W_i = \lambda_i f_1 \Big/ \pi a \tag{51}$$

$$\gamma_i = \lambda_i / \pi a \tag{52}$$

Since Rayleigh resolution criteria cannot be applied to the present case, the 1/e amplitude is arbitrarily chosen as the resolution limit.

From above discussion one may conclude:

- FOV and the intensity envelope of image plane may not be affected by the pump beam intensity distribution.
- The optical transfer function of the Fourier space configuration system depends heavily on the pump beam intensity distribution. A multimode pump beam (diverging pump beam), therefore, degrades resolution of the Fourier space configuration upconverter.

IV. UPCONVERSION EFFICIENCY

Conversion efficiency of the upconversion process has been measured and compared to a theoretical calculation based on the plane wave theory by several authors[9, 10, 11]. Measured efficiency, the conversion efficiency formula used for checking their results, and parameter values such as SHG d coefficients are inconsistent among investigators. In this section, an attempt will be made to clarify some of the confusion by considering:

- Proustite SHG d coefficients
- Experimental measurement of upconversion efficiency under controlled experimental conditions

A. PROUSTITE SHG d COEFFICIENTS

The only reported measurement of SHG d_{31} coefficients of proustite was performed by K. H. Hulme et al by comparing SHG of 1.152 μm with proustite to SHG with $LiNbO_3$ along the crystallographic X-axis[12]. The ratio $|d_{22}|/|d_{31}|$ of proustite was determined by Hulme et al by the frequency summing technique[12]. Their measurement did not determine the absolute signs of the coefficients. Their measured results are

$$\left|d_{31}^{P}\right| = 2.6\left|d_{31}^{LN}\right|$$
$$\left|d_{22}^{P}/d_{31}^{P}\right| = 1.6 \pm 0.1 \qquad (53)$$

The inconsistency in proustite d_{31} is resulted from the spread in $LiNbO_3$ d_{31} coefficient reported in the literature as shown below.

G. Boyd[13]

$$d_{31}^{(LN)} = (10.6 \pm 1.0)\, d_{36}^{(KDP)}$$

R. Miller and Savage[14]

$$d_{31}^{(LN)} = (11.9 \pm 1.7)\, d_{36}^{(KDP)}$$

Bjorkholm[15, 16]

$$d_{31}^{(LN)} = (10.9 \pm 1.7)\, d_{36}^{(KDP)}$$

Byer and Harris[17]

$$d_{31}^{(LN)} = 11.0\, d_{14}^{(KDP)} = 10.6\, d_{36}^{(KDP)}$$

Careful review of the above reported measurements indicates that Bjorkholm's measurement seems more accurate than others.

Using Jerphagnon and Kurtz[18] and Francois[19] measurement on d_{36} of KDP crystal,

$$d_{36}^{(KDP)} = 1.67 \times 10^{-9} \text{ esu}$$

and Bjorkholm's $d_{31}^{(LN)}$ one finds

$$\left|d_{31}^{(P)}\right| = 28.4\, d_{36}^{(KD)} = 42.6 \times 10^{-9} \text{ esu}$$
$$\left|d_{22}^{(P)}\right| = 45.5\, d_{36}^{(KDP)} = 68.2 \times 10^{-9} \text{ esu} \qquad (54)$$

Hulme[12] et al gave estimated d coefficients from their measurement as

$$\left|d_{22}^{(P)}\right| = 50\, d_{36}^{(KDP)} = 75 \times 10^{-9} \text{ esu}$$
$$\left|d_{31}^{(P)}\right| = 30\, d_{36}^{(KDP)} = 45 \times 10^{-9} \text{ esu} \qquad (55)$$

The reason for this modification from experimental results was not given by Hulme.

Boggett[20] et al reported the effective d coefficient of Type I phase matched proustite by measuring doubled 10.6 μm output power. Their results for $\theta_m = 22.5^o$.

$$d_{eff} = 60\, d_{36}^{(KDP)}$$

is higher than the calculated value based on Hulme's estimated d coefficients $d_{22}^{(P)} = 50\, d_{36}^{(KDP)}$ and $d_{31}^{(P)} = 30\, d_{36}^{(KDP)}$. If one solves the equation

$$d_{eff} = d_{22} \cos \theta_m + d_{31} \sin \theta_m$$

which applies to Type I phase matching, assuming $d_{32}/d_{31} = 1.6$ for proustite, one finds $d_{31}^{(P)} = 32.2\ d_{36}^{(KDP)}$ from the Boggett measurement. Boggett's result is very close to the Hulme's estimated d_{31} value.

The values $d_{22} = 68.2 \times 10^{-9}$ esu and $d_{31} = 42.6 \times 10^{-9}$ esu will be used for following system performance calculation, although Hulme's estimated d coefficients are widely adapted by other workers.

The choice is dictated by the conversion efficiency measurements performed at AIL. The result of the most recent conversion efficiency measurement is presented in paragraph B.

B. CONVERSION EFFICIENCY MEASUREMENTS

The main purpose of the experiment is to assess the achievable conversion efficiency of a practical image upconverter as compared to the theoretical estimate. The experimental conditions for efficiency measurements must be carefully controlled in order that the experimental results can be meaningfully compared to the theory.

Conversion efficiency of the experimental model was measured with TEM_{oo} mode signal beam and TEM_{oo} mode pump beam. The upconverted signal was detected by a low noise S1 photomultiplier with accurately calibrated quantum efficiency. Optical efficiency of optical components such as interference filter, optical windows, and the beam combining dichroic mirror were carefully calibrated. The pump beam was chopped with a duty factor of one quarter to prevent excessive crystal surface oxidation.

The input/output linearity was checked so that an efficiency measurement was taken within the dynamic range of the system. Figure 14 shows the plot of input CO_2 power versus the upconverted signal induced photoelectron at the photocathode. The observed power upconversion efficiency is calculated by

$$\eta_u = \frac{N_s\, hC}{\eta_p d\, P_{ir}\, \lambda_s} \tag{56}$$

where

N_s = photoelectron flux

η_p = quantum efficiency of the photomultiplier

h = Planck's Constant

C = velocity of light

λ_s = wavelength of upconverted signal

P_{ir} = IR input power

d = duty factor of light chopper

Using the following values:

$d = 0.25$

$\frac{hC}{\lambda_s} = 2.05 \times 10^{-19}$ Joules for $\lambda_s = 0.967\ \mu m$

$\eta_p = 9 \times 10^{-4}$

$N_s = 4 \times 10^5$ Hz

$P_{ir} = 0.09$ W

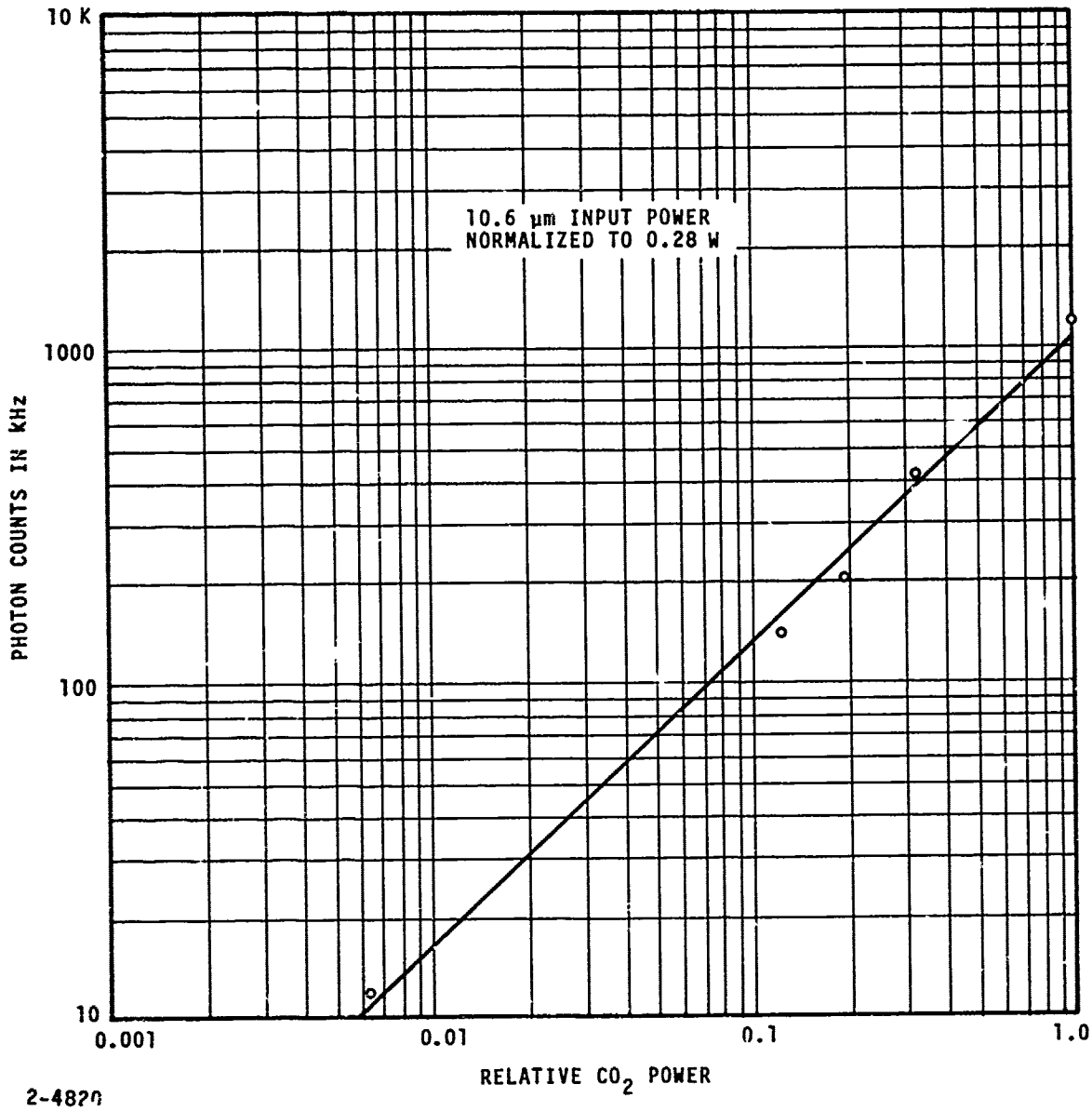

FIGURE 14. UPCONVERSION LINEARITY PHOTON COUNTS VERSUS RELATIVE CO_2 POWER

the measured system peak power conversion efficiency is 4.05×10^{-9} which is approximately one third of the theoretical estimated efficiency of 1.45×10^{-8} calculated by the expression

$$\eta = \frac{104.44\, d_{eff}^{\,2}\, \ell^2\, P_p\, t_{op}}{n_i\, n_s\, n_p\, \lambda_s^2\, (A_p + A_i)} = 2.162 \times 10^{-6} \frac{t_{op}\, \ell^2\, P_p}{(A_p + A_i)} \qquad (57)$$

where

P_p = pump power in watts

ℓ = interaction length in cm

n_ℓ = indices of refraction at (ℓ = i, p, s)

A_p = pump beam area in cm^2

A_i = IR beam area in cm^2

t = optical transmission of the experimental model

Parameter values used in the efficiency estimate are:

$d_{eff} = d_{22} \cos \theta_m = 68 (\cos 20^o) \times 10^{-9}$ esu $= 64 \times 10^{-9}$ esu

$n_i = 2.68$

$n_p = 2.817$

$n_s = 2.804$

$\ell = 0.6$ cm

$\lambda_s = 0.967\ \mu m$

$A_p = 1.13\ cm^2$ (beam diameter = 1.2 cm)

$A_i = 0.783\ cm^2$ (beam diameter = 1 cm)

$P_p = 4.8\ W$

$t_{op} = 7.44 \times 10^{-3}$

The most probable cause for the discrepancy between the measured efficiency and the prediction based on equation (57) is the phase mismatch due to the beam divergence. Equation (57) was derived for the case of perfectly phase matched interaction of two near-field Gaussian beams. Other factors affecting efficiency reduction are the beam walk-off, the crystal birefringence, and the crystal absorption.

System conversion efficiency under the experimental condition that nearly realizes the analytical model was measured. The measured conversion efficiency is approximately a factor of 1.75 less than the theoretical prediction. In this measurement the 10.6 μm beam was spatially filtered by a small pinhole placed at beam center. The filtered 10.6 μm wave front is very close to plane wavefront. Beam divergence effect is minimized by aligning the optics so that the interaction of IR waves with the pump waves is limited to the center of the pump beam.

Generally, the conversion efficiency formula used for the system calculation is different from equation (57). The generally accepted formula is[21, 22]

$$\eta = \frac{52.22\, d_{eff}^2\, \ell^2\, t_{op}\, P_p}{n_i\, n_s\, n_p\, \lambda_s^2\, A_p} \qquad (58)$$

which is obtained under the assumption of uniform intensity pump and $A_p >> A_i \approx A_s$.

The measured conversion efficiency with a small IR signal beam described here is 1.75 times lower than the theoretical estimate based on equation (57), but is within 15 percent of the estimate based on equation (58). It must, however, be noted that the measured conversion efficiency is the peak efficiency, since the interaction takes place at the center of pump beam, where the power density is the highest. Reduction in the efficiency at the skirt of the pump beam is expected.

From the experiments described and considerations made, it seems reasonable to conclude that power conversion efficiency estimated by equation (58) can be practically achieved at the center of FOV of the upconverter.

V. PLANS FOR EXPERIMENTS AND ANALYTICAL STUDIES FOR THE REMAINDER OF THE PROGRAM

The experimental effort for the remainder of the program will be directed toward:

- Optimization of a pulse gated image upconverter system and measurement of its operating characteristics such as conversion efficiency, resolving power, etc.
- Crystal damage experiments due to a high power pulse pump with moderate repetition rate.
- Measurement of thermal conductivity proustite.
- Image upconversion experiments with diffuse objects.
- Experimental verification of the crystal birefringent effect on the line spread function

The following areas will be studied analytically:

- Effect of pump beam intensity distribution on the image intensity envelope for the non-Fourier space configured upconverter.
- Accurate conversion efficiency calculation of the image space configuration image upconverter.
- System design calculation of the range gated image upconverter.
- Estimation of thermal detuning due to pump absorption.

REFERENCES

1. W. Chiou and F. Pace, "Research on Imaging Properties of Optical Parametric Upconverters," Final Report, AIL Report 8585-1, July 1971.

2. W. Chiou, "Journal of Applied Physics," Vol 42, p 1985, 1971.

3. W. Chiou and F. Pace, "Applied Physics Letters," Vol 20, p 44, 1972.

4. R.A. Andrews, IEEE, "Journal of Quantum Electronics," Vol QE-6, p 68, 1970.

5. J.E. Midwinter, "Applied Physics Letters," Vol 12, p 68, 1968.

6. J. Warner, "Applied Physics Letters," Vol 13, p 360, 1968.

7. J.F. Weller and R.A. Andrews, "Opto-Electronics," Vol 2, p 171, 1970.

8. J.W. Goodman, Introduction to Fourier Optics, McGraw-Hill, 1968.

9. J. Midwinter and J. Warner, "Journal of Applied Physics," Vol 38, p 519, 1967.

10. R.F. Lucy, "Applied Optics," Vol 11, p 1329, 1972.

11. D.C. Hanna, "Optics Communication," Vol 4, p 300, 1971.

12. K.F. Hulme, "Applied Physics Letters," Vol 10, p 133, 1967.

13. G. Boyd, "Applied Physics Letters," Vol 5, p 234, 1964.

14. R. Miller and E. Savage, "Applied Physics Letters," Vol 9, p 169, 1966.

15. J. Bjorkholm, IEEE, "Journal of Quantum Electronics," Vol QE-4, p 970, 1968.

16. J. Bjorkholm, IEEE, "Journal of Quantum Electronics," Vol QE-5, p 260, 1969.

17. R. Byer, "Physical Review," Vol 168, p 1064, 1968.

18. J. Jerphagnon and S. Kurtz, "Physical Review B," Vol 1, p 1739, 1970.

19. G.E. Francois, "Physical Review," Vol 143, p 597, 1966.

20. Boggett, "Applied Physics Letters," Vol 28A, p 33, 1968.

21. A.F. Milton, "Applied Optics," Vol 11, p 2311, 1972.

22. J. Warner, "Opto-Electronics," Vol 3, p 37, 1971.